Cell Reports Medicine

MPXV infection activates cGAS-STING signaling and IFN-I treatment reduces pathogenicity of mpox in CAST/EiJ mice and rhesus macaques

--Manuscript Draft--

Manuscript Number:	CR-MEDICINE-D-25-00032R2
Full Title:	MPXV infection activates cGAS-STING signaling and IFN-I treatment reduces pathogenicity of mpox in CAST/EiJ mice and rhesus macaques
Article Type:	Research Article
Keywords:	mpox virus, IFN-α/β, CAST/EiJ mice, rhesus macaques, splenomegaly, STING
Corresponding Author:	Jing Xue Chinese Academy of Medical Sciences Institute of Laboratory Animal Sciences Beijing, CHINA
First Author:	Lin Zhu
Order of Authors:	Lin Zhu
	Qi Liu
	Yongzhi Hou
	Baoying Huang
	Dong Zhang
	Zhe Cong
	Jianrong Ma
	Na Li
	Jiahan Lu
	Jingjing Zhang
	Lingyan Zhang
	Ting Chen
	Qiang Wei
	Jiangning Liu
	Wenjie Tan
	Jing Xue
Abstract:	The recent mpox outbreak underscores the urgent need for more accessible vaccines and treatments. However, the mpox virus (MPXV) clade IIb exhibits milder virulence and fails to develop typical pathological characteristics in mouse models. Herein, we found that CAST/EiJ mice infected intraperitoneally with MPXV clade IIb exhibited more efficient viral replication and experienced splenomegaly. Additionally, MPXV infection trigger the phosphorylation of STING, TBK1 and IRF3 in ex vivo bone marrow-derived macrophages from mice, and promote the transcription of IFN-β via the cGAS-STING pathway. Notably, IFN-β treatment significantly reduced viral replication and alleviating splenomegaly in MPXV-infected CAST/EiJ mice. In rhesus macaques, the clinically approved pegylated IFN alpha-2b treatment markedly reduced the severity of MPXV infection by alleviating skin lesions and lowering plasma viremia. These findings demonstrate that MPXV clade IIb activates the cGAS-STING pathway and highlight the potential of IFN-I treatment in CAST/EiJ mice and rhesus macaques for mpox.
Suggested Reviewers:	Jia Lu Wuhan Institute of Biological Products Co Ltd johnsonchau@163.com

Powered by Editorial Manager® and ProduXion Manager® from Aries Systems Corporation

	Chun Lu Nanjing Medical University clu@njmu.edu.cn
	Shuaiyao Lu Chinese Academy of Medical Sciences & Peking Union Medical College lushuaiyao-km@163.com
	Lu Lu Fudan University lul@fudan.edu.cn
	Feng Li Shanghai Public Health Clinical Center lifeng30511@shaphc.org
Opposed Reviewers:	Zheng Zhang zhangzheng1975@aliyun.com
Additional Information:	
Question	**Response**
Clinical trials Does your manuscript report clinical trial results?	No
Standardized datasets A list of datatypes considered standardized under Cell Press policy is available here. Does this manuscript report new standardized datasets?	Yes
Original code Does this manuscript report original computer code, algorithms, or computational models?	No
Reviewers must have free and anonymous access to these standardized datasets. Please provide dataset locations and instructions for access here. If applicable, include accession numbers and reviewer tokens. If you don't specify access information, your manuscript will not be sent to reviewers. Please consult these guides for more information: "Standardized datatypes, datatype-specific repositories, and general-purpose repositories recommended by Cell Press" and "How standardized datasets and original code accompany Cell Press manuscripts from submission through publication." Email us at cr-medicine@cell.com if you have any questions. as follow-up to "**Standardized datasets** A list of datatypes considered standardized under Cell Press policy is	The raw sequence data reported in this paper have been deposited in the Genome Sequence Archive in National Genomics Data Center, China National Center for Bioinformation / Beijing Institute of Genomics, Chinese Academy of Sciences under accession code of GSA: CRA023622. Accession numbers are listed in the key resources table. All the data shown in this paper are available from the lead contact upon reasonable request.

Powered by Editorial Manager® and ProduXion Manager® from Aries Systems Corporation

available here. Does this manuscript report new standardized datasets? "	

Powered by Editorial Manager® and ProduXion Manager® from Aries Systems Corporation

Mar 31, 2025
Editor-in-Chief
Cell Reports Medicine

Dear Dr. Yu,

We are pleased to submit the revised manuscript entitled "**MPXV infection activates cGAS-STING signaling and IFN-I treatment reduces pathogenicity of mpox in CAST/EiJ mice and rhesus macaques**" (Manuscript Number: CR-MEDICINE-D-25-00032) for further consideration in ***Cell Reports Medicine***. We have carefully addressed these specific issues, providing detailed point-by-point responses as follows.

- Please submit the main text containing the main figure legends and STAR methods as a Word document.
  Response: the main figure legends and STAR methods are included in the main text.
- Please submit the main manuscript figures as individual high-resolution files (TIF or high-resolution PDF). For more information, please view our Figure Guidelines.
  Response: the main manuscript figures are submitted individually as a high-resolution TIF files.
- Please carefully check STAR Methods as this part of the manuscript will not be copyedited.
  Response: STAR Methods are checked carefully.
- **Social Media:** We would like to promote your paper via Social Media. Please have a look at Cell's WeChat official account and let me know if you want to highlight your paper to Chinese readership.
  Response: We want to highlight our paper to Chinese readership.
- Please ensure that there are no priority claims in the paper (including new, novel, unique, 'the first' and other such phrases) or in the title, abstract and highlights of the paper.
  Response: Confirmed.
- Please make sure that the summary is written in the present tense and less than 150 words.
  Response: Adjusted as required.
- Figure legends should include information on biological and technical replicates if applicable.
  Response: the number of independent experiments were provided.
- Please submit the Supplemental information as a single PDF file. The supplemental section should be organized so that the relevant figure legend is placed beneath each Supplementary figure. The text should be Times New Roman (10 point) with single (left) justification of all text in the Supplemental document.
  Response: The supplemental information has been adapted as required and submitted as a single PDF

file.

- Please remove supplementary figures (.tif file) from the submission.
  Response: The TIF files of supplementary figures have been removed.

- Each Supplemental figure or table should be linked to at least one main-text figure or table, and/or to STAR Methods. This is indicated in the legend for the Supplemental figure; for example, "Figure S1. Flies lacking YFG do not exhibit changes in grooming behavior. Related to Figures 1 and 3." Every Supplemental figure must be cited at least once in the main text.
  Response: Every Supplemental figure and table have been cited in the main text.

- There is currently no graphical abstract, highlights, or eTOC summary. Please ensure the graphical abstract is the correct size and shape (1200 pixels square at 300 dpi), avoids field-specific abbreviations and that any text included can be read at final size. Please refer to our author guidelines for information on these items and our graphical abstract guidelines for more details and recommendations. Please also ensure that the highlights and eTOC summary should be written in present tense and submitted as a separate Word document.
  Response: Graphical abstract, highlights, and eTOC summary have been provided as request.

- We encourage you to try our Cell Press BioRender pilot to help you design a graphical abstract that meets our production requirements. *This will likely* ***reduce corrections requests and the time until formal acceptance.*** To access Biorender for Cell Press, please follow these simple steps: create an account using the Biorender portal, start a new illustration, enter your manuscript number (CR-MEDICINE-D-XX-XXXXX), and select the illustration size (Graphical Abstract). Online support from BioRender will be available for any questions if needed.
  Response: Graphical abstract is done by Biorender software.

- Data and Code Availability. It consists of three bulleted sections. Each section must be present.
  - Code: It is not clear if your paper reports custom computer code. If it does, your code must either be deposited in a repository that mints DOIs or included within the Supplemental Information before I can accept your paper. A list of repositories we endorse can be found here: https://www.cell.com/star-authors-guide. If you choose to deposit your code, please ensure it is publicly accessible and record the DOI in the Software and Algorithms section of the Key Resources Table. If your study does not report custom code, you should clearly state this.
  - General Statement: We require that the final bullet point of the Data and Code Availability statement states: “Any additional information required to reanalyze the data reported in this work paper is available from the Lead Contact upon request.” Please revise this statement.

Response: The raw sequence data reported in this paper have been deposited in the Genome Sequence Archive in National Genomics Data Center, China National Center for Bioinformation / Beijing Institute of Genomics, Chinese Academy of Sciences under accession code of GSA: CRA023622. Accession numbers are listed in the key resources table. Any additional information required to reanalyze the data reported in this work paper is available from the Lead Contact upon request.

We would like to take this opportunity to express our sincere thanks to the reviewers who identified areas of the manuscript that needed corrections or modification. We also thank you for allowing us to resubmit a revised copy of the manuscript.

This manuscript has not been submitted or accepted elsewhere. We hope that the revised manuscript is accepted for publication in ***Cell Reports Medicine***. Thank you very much, and look forward for your positive response soon.

Yours sincerely,

Jing Xue, Ph.D.

Professor & Chair, Infectious Disease Research Center

Institute of Laboratory Animal Science, Chinese Academy of Medical Sciences

No. 5 Panjiayuan Nanli, Beijing 100021, P.R. China

Phone/Fax: +86 10 67779771

E-mail: xuejing@cnilas.org

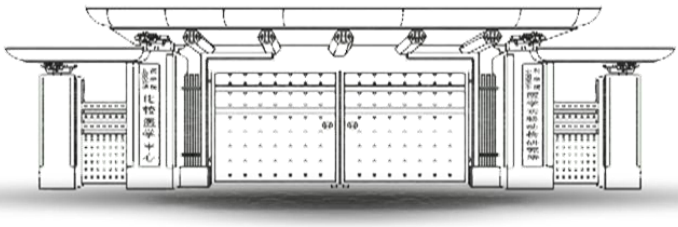

We have carefully addressed these specific issues, providing detailed point-by-point responses as follows.

- Please submit the main text containing the main figure legends and STAR methods as a Word document.
  Response: the main figure legends and STAR methods are included in the main text.
- Please submit the main manuscript figures as individual high-resolution files (TIF or high-resolution PDF). For more information, please view our Figure Guidelines.
  Response: the main manuscript figures are submitted individually as a high-resolution TIF files.
- Please carefully check STAR Methods as this part of the manuscript will not be copyedited.
  Response: STAR Methods are checked carefully.
- **Social Media:** We would like to promote your paper via Social Media. Please have a look at Cell's WeChat official account and let me know if you want to highlight your paper to Chinese readership.
  Response: We want to highlight our paper to Chinese readership.
- Please ensure that there are no priority claims in the paper (including new, novel, unique, 'the first' and other such phrases) or in the title, abstract and highlights of the paper.
  Response: Confirmed.
- Please make sure that the summary is written in the present tense and less than 150 words.
  Response: Adjusted as required.
- Figure legends should include information on biological and technical replicates if applicable.
  Response: the number of independent experiments were provided.
- Please submit the Supplemental information as a single PDF file. The supplemental section should be organized so that the relevant figure legend is placed beneath each Supplementary figure. The text should be Times New Roman (10 point) with single (left) justification of all text in the Supplemental document.
  Response: The supplemental information has been adapted as required and submitted as a single PDF file.

- Please remove supplementary figures (.tif file) from the submission.
  Response: The TIF files of supplementary figures have been removed.

- Each Supplemental figure or table should be linked to at least one main-text figure or table, and/or to STAR Methods. This is indicated in the legend for the Supplemental figure; for example, "Figure S1. Flies lacking YFG do not exhibit changes in grooming behavior. Related to Figures 1 and 3." Every Supplemental figure must be cited at least once in the main text.
  Response: Every Supplemental figure and table have been cited in the main text.

- There is currently no graphical abstract, highlights, or eTOC summary. Please ensure the graphical abstract is the correct size and shape (1200 pixels square at 300 dpi), avoids field-specific abbreviations and that any text included can be read at final size. Please refer to our author guidelines for information on these items and our graphical abstract guidelines for more details and recommendations. Please also ensure that the highlights and eTOC summary should be written in present tense and submitted as a separate Word document.
  Response: Graphical abstract, highlights, and eTOC summary have been provided as request.

- We encourage you to try our Cell Press BioRender pilot to help you design a graphical abstract that meets our production requirements. *This will likely* ***reduce corrections requests and the time until formal acceptance.*** To access Biorender for Cell Press, please follow these simple steps: create an account using the Biorender portal, start a new illustration, enter your manuscript number (CR-MEDICINE-D-XX-XXXXX), and select the illustration size (Graphical Abstract). Online support from BioRender will be available for any questions if needed.
  Response: Graphical abstract is done by Biorender software.

- Data and Code Availability. It consists of three bulleted sections. Each section must be present.
  - Code: It is not clear if your paper reports custom computer code. If it does, your code must either be deposited in a repository that mints DOIs or included within the Supplemental Information before I can accept your paper. A list of repositories we endorse can be found here: https://www.cell.com/star-authors-guide. If you choose to deposit your code, please ensure it is publicly accessible and record the DOI in the Software and Algorithms section of the Key Resources Table. If your study

does not report custom code, you should clearly state this.

- General Statement: We require that the final bullet point of the Data and Code Availability statement states: "Any additional information required to reanalyze the data reported in this work paper is available from the Lead Contact upon request." Please revise this statement.

Response: The raw sequence data reported in this paper have been deposited in the Genome Sequence Archive in National Genomics Data Center, China National Center for Bioinformation / Beijing Institute of Genomics, Chinese Academy of Sciences under accession code of GSA: CRA023622. Accession numbers are listed in the key resources table. Any additional information required to reanalyze the data reported in this work paper is available from the Lead Contact upon request.

Click here to access/download
Graphical Abstract
Graphical Abstract.pdf

Click here to access/download
Graphical Abstract
Publication License Mar-30-2025.pdf

Manuscript Click here to view linked References

MPXV infection activates cGAS-STING signaling and IFN-I treatment reduces pathogenicity of mpox in CAST/EiJ mice and rhesus macaques

Running Title: IFN-I reduces pathogenicity of mpox in mice and macaques

Lin Zhu[1,4], Qi Liu[1,4], Yongzhi Hou[1,4], Baoying Huang[2,4], Dong Zhang[1], Zhe Cong[1], Jianrong Ma[1], Na Li[1], Jiahan Lu[1], Jingjing Zhang[1], Lingyan Zhang[1], Ting Chen[1], Qiang Wei[1,3], Jiangning Liu[1], Wenjie Tan[2,*], and Jing Xue[1,3,5,*]

[1]NHC Key Laboratory of Human Disease Comparative Medicine, Beijing Key Laboratory for Animal Models of Emerging and Remerging Infectious Diseases, Institute of Laboratory Animal Science, Chinese Academy of Medical Sciences and Peking Union Medical College, Beijing, 100021, China

[2]NHC Key Laboratory of Biosafety, National Key Laboratory of Intelligent Tracking and Forecasting for Infectious Diseases, National Institute for Viral Disease Control and Prevention, Chinese Center for Disease Control and Prevention, Beijing, 102206, China

[3]State Key Laboratory of Respiratory Health and Multimorbidity, Key Laboratory of Pathogen Infection Prevention and Control (Peking Union Medical College), Ministry of Education, Institute of Laboratory Animal Science, Chinese Academy of Medical Sciences, Beijing, 100021, China

[4]These authors contributed equally

[5]Lead contact

[*]Correspondence to: Jing Xue (xuejing@cnilas.org), Wenjie Tan (tanwj@ivdc.chinacdc.cn)

Summary

The recent mpox outbreak underscores the urgent need for more accessible vaccines and treatments. However, the mpox virus (MPXV) clade IIb exhibits milder virulence and fails to develop typical pathological characteristics in mouse models. Herein, we found that CAST/EiJ mice infected intraperitoneally with MPXV clade IIb exhibited more efficient viral replication and experienced splenomegaly. Additionally, MPXV infection trigger the phosphorylation of STING, TBK1 and IRF3 in *ex vivo* bone marrow-derived macrophages from mice, and promote the transcription of IFN-β via the cGAS-STING pathway. Notably, IFN-β treatment significantly reduced viral replication and alleviating splenomegaly in MPXV-infected CAST/EiJ mice. In rhesus macaques, the clinically approved pegylated IFN alpha-2b treatment markedly reduced the severity of MPXV infection by alleviating skin lesions and lowering plasma viremia. These findings demonstrate that MPXV clade IIb activates the cGAS-STING pathway and highlight the potential of IFN-I treatment in CAST/EiJ mice and rhesus macaques for mpox.

Keywords: mpox virus, IFN-α/β, CAST/EiJ mice, rhesus macaques, splenomegaly, STING.

Introduction

Mpox, a zoonotic disease formerly known as monkeypox, is caused by the mpox virus (MPXV), an enveloped double-stranded DNA virus belonging to the *Orthopoxvirus* genus of the *Poxviridae* family[1,2]. The discovery of mpox in macaques date back to 1958, and its identification as a human pathogen occurred in the Congo region of Africa in 1970[3,4]. Initially believed to be an endemic zoonotic disease primarily found in Central and West Africa, mpox has become an alarming global concern since May 2022, with over 129,172 cases reported across 130 countries, predominantly among men who have sex with men. Considering the global threat, mpox was declared a public health emergency of international concern (PHEIC) by the World Health Organization (WHO) on July 23, 2022 and August 14, 2024, respectively[5,6]. The outbreak since 2022 is attributed to the West African B.1 lineage clade IIb of mpox strains, with a mortality rate of less than 1%, which is lower than that of clade I strains, which have mortality rates of up to 10%. Importantly, clade IIb strains have exhibited extensive human-to-human spread[1,7].

Animal models, especially mouse models, play a crucial role in studying viral pathogenesis, vaccine development, and drug testing. Among the 38 inbred strains of mice screened for MPXV susceptibility, only three-derived strains (CAST/EiJ, MOLF/EiJ, and PERA/EiJ) are highly susceptible to MPXV infection[8]. Among these susceptible mouse strains, the CAST/EiJ mouse strain, derived from wild *Mus musculus castaneus* trapped in Thailand, is the most sensitive to MPXV. However, this mice model does not develop skin lesions or rashes[8-11]. Lower levels of natural killer cells (a deficient gamma interferon response) may contribute to their susceptibility to MPXV, and IL-15-treated CAST/EiJ mice are protected against lethal challenge with vaccinia virus (VACV) or MPXV[9,12].

Warner *et al*. reported that daily oral gavage of tecovirimat (TPOXX) significantly reduced viral titers in tissues from MPXV-infected CAST/EiJ mice[13]. Recently, the effectiveness of the MPXV mRNA vaccine (BNT166) has also been evaluated in CAST/EiJ mice[14]. Weight loss and lethal infection were observed in CAST/EiJ mice infected with the MPXV clade I and IIa strains, but not with the MPXV clade IIb strain[7]. Despite the detection of viral replication, typical pathological manifestations are still absent in CAST/EiJ mice infected with the MPXV clade IIb strain[14]. In addition to CAST/EiJ mice, which serve as effective models for MPXV infection, nonhuman primates develop mpox-like rashes, skin inflammation, and sustained viremia following MPXV challenge, making them ideal models for studying mpox pathogenesis[6,14-16].

Cells sense the presence of invading pathogens via pattern-recognition receptors (PRRs), which are germ line-encoded molecules that recognize pathogen-associated molecular patterns (PAMPs). Cytosolic double-stranded DNA (dsDNA) can be detected by multiple PRRs, with their importance varying depending on the cell type[17]. Among these PRRs, cyclic guanosine monophosphate (GMP) adenosine monophosphate (AMP) synthase (cGAS) serves as a cytosolic DNA sensor that recognizes viral dsDNA and generates cyclic GMP-AMP (cGAMP). This cGAMP then binds to the adaptor protein stimulator of interferon genes (STING) located in the endoplasmic reticulum[18,19]. Subsequently, STING undergoes homodimerization and acts as a scaffold to recruit TANK-binding kinase 1 (TBK1) for the phosphorylation and activation of interferon regulatory factor 3 (IRF3), leading to the induction of type I interferon (IFN-I, including IFN-α and IFN-β)[20-22]. Therefore, targeting the STING-TBK1-IRF3-IFN-I axis is an extremely critical strategy for host cells to defend against DNA viruses. Previous studies

have demonstrated that some viruses belonging to the *Poxviridae* family can activate the cGAS-STING pathway. Modified vaccinia virus Ankara (MVA) infection elicits IFN-I production via the cGAS-STING pathway in murine conventional dendritic cells (cDCs) but not in plasmacytoid dendritic cells (pDCs)[23]. Ectromelia virus (ECTV), a mouse-specific pathogen that causes mousepox, can induce IFN-I production in L929 and RAW264.7 cells via the cGAS-STING pathway[24]. In addition, virulent VACV strains or other virulent poxviruses that inhibit DNA sensing by preventing STING activation have also been reported[25-27]. Considering the MPXV epidemic strain clade IIb has relatively milder virulence compared to clade I, it remains unclear whether MPXV, particularly clade IIb strains, can stimulate IFN-I production via the STING-TBK1-IRF3 axis. Although Johnston *et al*. demonstrated that IFN-β inhibits MPXV clade I replication *in vitro*[28], its inhibitory effect *in vivo* remains unknown.

In this study, we used CAST/EiJ mice as models to evaluate two routes of inoculation for MPXV clade IIb. Our findings indicated that the intraperitoneal (*i.p.*) route of infection demonstrated superior efficacy compared to the intranasal (*i.n.*) route. Additionally, we used *ex vivo* bone marrow-derived macrophages (BMDMs) derived from CAST/EiJ mice to investigate the effect of MPXV clade IIb infection on the activation of the cGAS-STING signaling pathway, and to explore the protective role of IFN-I (including IFN-α and IFN-β) in CAST/EiJ mice and rhesus macaques against MPXV challenge.

Results

MPXV clade IIb infection via the intraperitoneal route in CAST/EiJ mice results in higher viral replication than the intranasal route

In 2022, Huang *et al.* identified and isolated the first MPXV strain (MPXV-B.1-China-C-Tan-CQ01) in mainland China. This strain belongs to the West African lineage clade and shares high genetic similarity with strain collected from Germany on June 21, 2022 (GISAID ID: EPI_ISL_13889435)[29,30]. Herein, we aimed to study the pathogenicity of MPXV-B.1-China-C-Tan-CQ01 strain (MPXV clade IIb strain) in a suitable mouse model. Americo *et al*. previously reported that CAST/EiJ mice are susceptible to MPXV and subsequently showed that the virulence of the MPXV clade I and clade IIa is greater than that of the MPXV Clade IIb[7,8]. To systematically assess the infectivity of MPXV-B.1-China-C-Tan-CQ01, we inoculated 48 CAST/EiJ mice with MPXV at a dose of 1.0×10^6 median tissue culture infectious doses ($TCID_{50}$) via the intraperitoneal (*i.p.*) or intranasal (*i.n.*) route. The mice were euthanized at 0, 4, 7, 11, 21, and 28 days post infection (dpi) and the viral loads in the plasma and tissues were analyzed[6,13,31] (Figure. 1A). No weight loss and death were observed in CAST/EiJ mice infected with MPXV clade IIb via either the *i.p.* or *i.n.* route (Figures 1B and 1C). Furthermore, plasma viral DNA was assessed by qualitative PCR (qPCR) assays targeting the MPXV-specific F3L gene at 0, 4, 7, 11, 21, and 28 dpi. Viral DNA was detectable on days 4 and 7 after *i.p.* and *i.n.* route infection, peaking on day 4 (Figure1D). The peak viral loads were 5.41 $\log_{10}$ copies/ml (range 4.85-6.51) for the *i.p.* route and 4.13 $\log_{10}$ copies/ml (range 3.91-4.34) for the *i.n.* route (Figure 1D). However, no viruses were detected in the plasma on days 11, 21, or 28 after infection, regardless of whether the infection route was *i.p.* or *i.n.* (Figure 1D). Moreover, we compared the plasma viral loads between male and female mice after mixing samples from

CAST/EiJ mice infected via the *i.p.* route at 4 and 7 dpi. Although the plasma viral loads in male mice were slightly greater than those in female mice, the difference was not statistically significant (Figure. S1A).

Next, the number of copies of the viral genome present in various organs of the mice was determined. Four days after infection through the *i.p.* and *i.n.* routes, the virus was detectable in tissues such as the heart, liver, spleen, lungs, kidneys, brain, intestines, stomach, and lymph nodes (inguinal lymph nodes). Among these, the highest viral loads were observed in the spleen and intestines, reaching approximately 7.0 $\log_{10}$ copies/μg DNA after 4 days of *i.p.* infection (Figures 1E and S1B). Conversely, the viral load in the lungs was greater (approximately 4.0 $\log_{10}$ copies/μg DNA) at 4 days after *i.n.* infection. Additionally, the intestines exhibited the greatest viral loads, approximately 5.0 $\log_{10}$ copies/μg DNA, after seven days of *i.n.* infection (Figures 1E and S1C). Moreover, viral titers in the plasma and tissues were quantified using the $TCID_{50}$ assay. For the *i.p.* route, the average viral titers in the plasma on day 4 were approximately 4.0 $\log_{10}$ $TCID_{50}$/ml, which was significantly higher than those observed with the *i.n.* route (Figure 1F). This discrepancy may reflect a less robust systemic infection via the *i.n.* route or limitations in the sensitivity of the viral titer assay. Similarly, the average viral titers in liver (5.6 $\log_{10}$ $TCID_{50}$/g), spleen (6.9 $\log_{10}$ $TCID_{50}$/g), kidneys (6.0 $\log_{10}$ $TCID_{50}$/g), intestines (5.7 $\log_{10}$ $TCID_{50}$/g), and stomach (4.9 $\log_{10}$ $TCID_{50}$/g) for the *i.p.* route on day 4 were significantly higher than those for the *i.n.* route (Figure 1G). However, the viral titers in the heart, lung, and lymph nodes showed no significant differences between the two routes (Figure 1G). Unlike other tissues, the average viral titers in lung tissue via the *i.p.* route (4.7 $\log_{10}$ $TCID_{50}$/g) were slightly lower than those via the *i.n.* route (5.3 $\log_{10}$ $TCID_{50}$/g), although

this difference was not statistically significant (Figure 1G). We have expanded our study to investigate the effects of higher MPXV doses in CAST/EiJ mice, administering escalating concentrations of 1×10^6, 3×10^6, and 1×10^7 $TCID_{50}$ via *i.p.* route. Our findings indicate that higher MPXV doses of 3×10^6 $TCID_{50}$ and 1×10^7 $TCID_{50}$ had no significant impact on body weight or survival in CAST/EiJ mice (Figure S2). Taken together, these findings indicate that the CAST/EiJ mice were susceptible to MPXV clade IIb infection and that the *i.p.* route was more effective than the *i.n.* route.

CAST/EiJ mice infected with MPXV clade IIb via the intraperitoneal route exhibit splenomegaly

Typical symptoms of mpox-infected patients include fever, headache, muscle pain, lymphadenopathy, and characteristic rashes that progress from papules and vesicles to pustules and eventually crust over and heal[32]. No skin lesions were found in MPXV-infected CAST/EiJ mice via either the *i.p.* or the *i.n.* route (data not shown). Upon euthanasia, CAST/EiJ mice infected with MPXV clade IIb via the *i.p.* or *i.n.* route displayed mild regional lymphadenopathy (Figure S1D). Furthermore, the results of gross pathology showed the increase in splenic size (Figure 2A) and splenic weight (expressed as a percentage of body weight) (Figure 2B) in MPXV clade IIb-infected CAST/EiJ mice via the *i.p.* route at 4, 7 and 11 dpi, while no significant changes were observed in the lung size (Figure S3A) or lung weight (Figure S3B) of MPXV clade IIb-infected CAST/EiJ mice via the *i.n.* route. Moreover, we performed histological studies on the spleen and lung tissue of MPXV clade IIb-infected CAST/EiJ mice via the *i.p.* route. Histological analysis revealed that MPXV clade IIb infection in CAST/EiJ mice via *i.p.* route induced splenic pathological changes, characterized by hyperplasia of the white pulp with prominent

germinal centers, along with the increased extramedullary hematopoiesis and macrophages infiltration in the red pulp (Figure 2C). Immunohistochemistry (IHC) analysis further confirmed that MPXV positive staining in the red pulp, with a significant increase in macrophages in the red pulp compared to uninfected control (Figures 2D and 2E). However, inflammation was not observed in the lungs of either the infected or non-infected CAST/EiJ mice (Figure. S3C).

We further analyzed the quantity and proportion of immune cells in the spleen tissues of CAST/EiJ mice before and after infection. As shown in Figure 2F, MPXV clade IIb infection led to an increase in the numbers of B cells, T cells, NK cells and cDCs (conventional DCs) among the splenic immune cells. Additionally, MPXV clade IIb infection resulted in a decreased proportion of $CD4^+$ T cells (68.0% vs. 59.3%) and an increased proportion of $CD8^+$ T cells (28.8% vs. 35.5%) within the splenic T cell population, significantly reducing the $CD4^+/CD8^+$ T cell ratio (Figure 2G). These findings suggest that splenomegaly may be a characteristic pathological manifestation in CAST/EiJ mice infected with MPXV clade IIb via the *i.p.* route.

We then conducted RNA-seq analysis of spleen transcriptomic profiles from naïve and MPXV-infected CAST/EiJ mice. Differential expression analysis using DESeq2 identified significant gene expression changes, with key differentially expressed genes highlighted (Figures S4A-S4C). Metascape enrichment analysis revealed that upregulated genes were enriched in cell cycle-related processes, response to virus or interferon, as well as antiviral pathways by interferon signaling (Figure S4D), implying an active immune response and cellular proliferation that may potentially contribute to the observed splenomegaly.

Increased IFN-β production by activating the cGAS-STING pathway in MPXV clade IIb-infected BMDMs

To determine whether MPXV can activate the cGAS-STING pathway in mouse-derived *ex vivo* cells, BMDMs were obtained from C57BL/6J and CAST/EiJ mice and infected with MPXV clade IIb (Figure 3A). As shown in Figure 3B, MPXV clade IIb infection induced the phosphorylation of STING, TBK1, and IRF3 in BMDMs from C57BL/6J and CAST/EiJ mice. Moreover, MPXV clade IIb infection promoted cGAMP concentration in BMDMs derived from C57BL/6J and CAST/EiJ mice, and cGAMP concentration were higher in BMDMs derived from CAST/EiJ mice than in C57BL/6J mice (Figure 3C). Additionally, MPXV infection led to increased production of IFN-β and its downstream genes, including CXCL10, ISG15, ISG56, CCL5, and IFIT2, in BMDMs from MPXV clade IIb-infected C57BL/6J and CAST/EiJ mice (Figures 3D and S5A-S5E).

Moreover, phosphorylated STING and TBK1 also accumulated in the cytoplasm of MPXV-infected cells and significantly colocalized with the MPXV A29 protein (Figures 3E-3H). In contrast, no phosphorylation of STING or TBK1 was detected in uninfected cells (Figures S6A and S6B). These collective results provide evidence for the activation of the cGAS-STING signaling pathway by MPXV clade IIb infection in BMDMs derived from C57BL/6J and CAST/EiJ mice.

To verify whether MPXV promotes IFN-β production via STING pathway, we first used the STING inhibitor H151 in MPXV-infected BMDMs. The results showed that the transcription of IFN-β (Figure 4A) and its downstream genes such as CXCL10, ISG15, ISG56, and CCL5 in BMDMs induced by MPXV could be significantly antagonized by

H151 (Figures 4B-4E). Then, *STING*-knockout THP-1 cells (Figure 4F) were used to investigate whether the effect of MPXV clade IIb on the transcription of IFN-β and its downstream genes is regulated by STING. As shown in Figures 4G and 4H, MPXV clade IIb infection promoted the transcription of IFN-β and its downstream genes (e.g., CXCL10, ISG15 and ISG56) in THP-1 cells, but failed to potentiate the transcription of IFN-β and its downstream genes in *STING*-knockout cells. Overall, these findings demonstrated that MPXV clade IIb promotes IFN-β production in a STING-dependent manner.

IFN-β treatment can efficiently suppress MPXV clade IIb replication and mitigate splenomegaly in CAST/EiJ mice

Since MPXV clade IIb can activate the production of IFN-β via cGAS-STING pathway, we investigated the impact of STING activator/inhibitor and IFN-β proteins in inhibiting viral replication. First, we examined the impact of different concentrations of the STING inhibitor H151 or the STING activator DMXAA on MPXV replication in BMDMs. Remarkably, DMXAA significantly inhibited MPXV clade IIb replication, while H151 promoted MPXV clade IIb replication (Figures 5A, 5B and S7A, S7B). Then, we examined the effect of the IFN-β protein on MPXV replication. Intriguingly, even very low concentrations of IFN-β (approximately 97.5 pg/ml) significantly inhibited MPXV replication in BMDMs (Figures 5C and S7C). These findings suggest that IFN-β protein and STING agonists can be used to inhibit MPXV clade IIb replication *in vitro*.

Furthermore, we conducted *in vivo* experiments in CAST/EiJ mice to evaluate the prophylactic and therapeutic efficacy of IFN-β against MPXV challenge. IFN-β (1 μg/mouse) was administered at various time points relative to MPXV infection via the *i.p.*

route: 3 hours before infection (MPXV/IFN-β -3h), 3 hours after infection (MPXV/IFN-β +3h), and 1 day after infection (MPXV/IFN-β +1d), with a control group receiving saline (MPXV/Saline). A second IFN-β dose was administered 2 days after the initial dose[33]. Mice were euthanized on day 4 post-infection, and MPXV loads were quantified in plasma and tissues (heart, liver, spleen, lung, and kidney) (Figure 5D). IFN-β treatment across all three groups caused no weight loss in CAST/EiJ mice (Figure 5E). Notably, while IFN-β administered 3 hours prior to infection most effectively reduced viral loads, treatments at 3 hours and 1 day post-infection also significantly mitigated splenomegaly and suppressed MPXV replication across all assessed tissues (Figure 5F-5H).

Peg-IFN alpha-2b treatment significantly reduces the pathogenicity of rhesus macaques against MPXV challenge

To evaluate IFN-I efficacy in a model that better represents human mpox, including development of lesions, we used rhesus macaques MPXV challenge model and the clinically used pegylated IFN alpha-2b (Peg-IFN alpha-2b). Six rhesus macaques were divided into two groups of three and received either a day 1 before MPXV infection (-1 dpi) and day 6 post MPXV infection (6 dpi) treatment with 60 μg Peg-IFN alpha-2b or mock saline via subcutaneous (*s.c.*) route. At day 0, all animals were challenged with MPXV via intravenous (*i.v.*) route and monitored for 28 days for disease symptoms including body temperature, weight loss, skin lesions and viremia[6,15,16] (Figure 6A). No significant change in body temperature was observed in the IFN alpha-2b-treated group, compared to a modest increase in body temperature at 7 days post MPXV infection in the saline-treated group (Figure 6B). As shown in Figure 6C, no significant changes in body

weight were observed in IFN alpha-2b treated groups throughout the MPXV IIb challenge observation period.

Clinical disease was evaluated by counting the number of skin lesions after MPXV challenge. In the saline-treated group, animals developed a median of 125 lesions per animal by 7 dpi (range 44-242), peaking at a median of 341 lesions by 10 dpi (range 268-462) over the entire body (Figure 6D). In contrast, Peg-IFN alpha-2b-treated animals only observed a median of 52 lesions (range 1-142) by 7dpi, 143 lesions (range 16-300) by 10 dpi, indicating robust clinical protection (Figure 6D). Plasma viral DNA in the Peg-IFN alpha-2b-treated groups was determined by quantitative reverse transcription polymerase chain reaction (qRT-PCR) assays following MPXV challenge. Viral loads in plasma were detectable at 4 dpi in the saline-treated group, with median DNA copies per milliliter on days 4, 7 and 10 were $10^{5.70}$, $10^{6.53}$, $10^{7.14}$, respectively (Figure 6E). In comparison, the median DNA copies per milliliter was significantly lower in the Peg-IFN alpha-2b-treated groups, at $10^{3.83}$, $10^{4.10}$, and $10^{4.99}$, respectively (Figure 6E), and an approximately 100-fold reduction in plasma viral loads compared to the control group. Collectively, these results showed that rhesus macaques treated with Peg-IFN alpha-2b offer robust but incomplete protection against MPXV challenge. Moreover, compared to pre-treatment baseline levels, the transcription levels of ISG-related genes (including ISG15, CXCL10 and IFIT2) in PBMC of rhesus monkeys were significantly increased during IFN α-2b treatment, followed by a marked decrease post-treatment (Figure S8), suggesting that dynamic changes in ISG expression may contribute to modulating mpox disease progression. Taken together, these findings suggest that IFN-I (IFN-β or IFN-α protein) play an important role in inhibiting MPXV replication and alleviating disease manifestations in small animal

models and non-human primates (NHPs), highlighting its potential as a therapeutic agent for mpox.

Discussion

Previous studies have shown that CAST/EiJ mice are susceptible to MPXV and have been used as a model for testing the efficacy of smallpox vaccines and antiviral drugs against MPXV[11,13,34]. However, systematic comparisons of different infection routes in CAST/EiJ mice, as well as tissue pathologies, have not been reported for MPXV, especially for the clade IIb strain. Here, we found that no weight loss and death were observed in CAST/EiJ mice infected with MPXV clade IIb via either the *i.p.* or *i.n.* route, consistent with previous reports[7,13]. We not only elucidated that the *i.p.* infection route was more effective than the *i.n.* infection route in CAST/EiJ mice (Figure 1), but also unexpectedly revealed that the *i.p.* route caused splenomegaly that can be used as a typical pathological manifestation of MPXV infection (Figures 2A-2C). Tang *et al*. reported that BALB/c mice can also be used as an infection model of MPXV, but only at extremely high infectious doses (infection with 20 μl of 2.24×10^8 PFU/ml MPXV via the *i.n.* route (4.48×10^6 PFU) combined with 480 μl of 2.24×10^8 PFU/ml MPXV via the *i.p.* route(1.0752×10^8 PFU))[35]. In addition, the viral loads in the lungs and spleen of BALB/c mice were significantly lower than those in CAST/EiJ mice (10^2 copies/ml vs. 10^7 copies/ml in the spleen and 10^4 copies/ml vs. $10^{5.3}$ copies/ml in the lungs at 4 dpi), although the initial infection dose was only 1.0×10^6 $TCID_{50}$ in CAST/EiJ mice. These results suggested that CAST/EiJ mice are more susceptible as MPXV infection models than are BALB/c mice.

The typical symptoms experienced by mpox patients include lesions and lymphadenopathy[4,36]. However, it is unclear whether the organs of MPXV-infected mice exhibit similar symptoms. In our study, utilizing a CAST/EiJ mouse infection model, we demonstrated that MPXV clade IIb infection via the *i.p.* route not only promotes mild lymphadenopathy but also induces splenomegaly, resulting in increased splenic size and weight at 4, 7 and 11 dpi (Figures 2A, 2B and S1D). Histological and IHC analysis revealed a significant increase in macrophages in the red pulp of MPXV clade IIb infected-CAST/EiJ mice compared to uninfected control (Figures 2C-2E). Our findings suggest that MPXV infection may contribute to splenomegaly via macrophage expansion in the red pulp, we cannot definitively attribute it solely to the virus without ruling out other immune-mediated effects. Further analysis of spleen cell suspensions showed an increase in the numbers of T cells, B cells, NK cells, and cDC cells, along with a significant reduction in the CD4/CD8 ratio among splenic T cells. Viallard *et al*. reported that expansion of the $CD8^+$ T cell compartment and the reversal of the $CD4^+/CD8^+$ T cell ratio are key contributors to splenomegaly[37]. Consistent with this, our study found that MPXV clade IIb infection in CAST/EiJ mice led to a decrease in the proportion of $CD4^+$ T cells, an increase in the proportion of $CD8^+$ T cells, and a reduction in the $CD4^+/CD8^+$ T cell ratio (Figure 2G), which may be the main cause of splenomegaly. Although viral loads were detectable in the lungs of CAST/EiJ mice following MPXV infection via *i.n.* and *i.p.* route, consistent with prior studies[7], no significant lung inflammation or gross pathological changes were observed. This may suggest that the viral loads achieved via the *i.n.* route is insufficient to trigger robust inflammatory responses in the lung tissue, potentially due to limited viral replication or dissemination in this model.

Our findings revealed that *ex vivo* BMDMs from CAST/EiJ and C57BL/6J mice exhibited activation of the cGAS-STING signaling pathway upon MPXV infection (Figures 3A-H). Additionally, MPXV employs its P2 protein to disrupt IFN production by binding KPNA2, thereby inhibiting IRF3 nuclear translocation via the nuclear localization signal (NLS)-dependent mechanism[38]. Prototypic poxvirus, such as virulent VACV strains Copenhagen and Western Reserve inhibit DNA sensing by preventing cGAS-STING activation through poxvirus immune nucleases (poxins), E3L and CCL4[25-27,39]. However, whether MPXV can active cGAS-STING signaling pathway has not been reported. Our findings revealed that *ex vivo* BMDMs from CAST/EiJ and C57BL/6J mice activate the cGAS-STING signaling pathway upon MPXV clade IIb infection. Therefore, it would be very interesting to investigate whether there is a correlation between the virulence differences of MPXV clades I, Ib, IIa, and IIb, and cGAS-STING activation. Since the clade IIb strain is currently the only MPXV strain available in China, the relationship between MPXV virulence and cGAS-STING activation requires further investigation once additional strains are obtained. In addition to promoting IRF3-mediated IFN-I synthesis, STING activation also amplifies IFN responses and bolsters host antiviral defense by engaging the NF-κB pathway. This occurs through IκB-α degradation, which activates NF-κB signaling and, in turn, stabilizes STING to enhance antiviral immunity[40,41]. Therefore, the potential involvement of STING-mediated NF-κB p65 activation in the antiviral response to MPXV warrants further exploration. Specifically, it would be intriguing to determine whether MPXV modulates host antiviral defenses by influencing NF-κB activity. Additionally, we observed colocalization of p-STING and p-TBK1 with MPXV A29, raising the possibility that A29 directly interacts with these phosphorylated proteins to

enhance cGAS-STING pathway activation. This is intriguing given that MPXV infection also increases cellular cGAMP levels, suggesting a dual mechanism of pathway stimulation potentially through A29-mediated binding and cGAMP-driven canonical signaling. Further studies are needed to confirm whether A29 serves as a viral effector that modulates STING-TBK1 activity and to delineate the precise molecular interactions involved.

As a significant component of innate immunity, IFN-I has a crucial impact on the control of viral infections by modulating the activities of associated immune cells[42]. Although IFN-β has been reported to inhibit the replication of MPXV-Zaire (clade I) in HeLa cells[28], there are no reports that MPXV (clade I) induces IFN-β production by activating STING. Therefore, it is unclear whether IFN-β can inhibit the replication of MPXV (clade IIb). Herein, we found that IFN-β not only suppressed MPXV (clade IIb) replication in BMDMs (Figure 5C) but also markedly inhibited the replication of MPXV in both plasma and tissues in CAST/EiJ mice (Figures 5G and 5H). Notably, IFN-β administration 3 hours prior to MPXV infection (MPXV/IFN-β -3h) most effectively suppressed MPXV replication in plasma and tissues, surpassing the efficacy of treatments at 3 hours (MPXV/IFN-β +3h) and 1 day (MPXV/IFN-β +1d) post MPXV infection. These findings suggest that early IFN-β administration maximizes its antiviral efficacy by limiting viral dissemination, while post-infection administration still conferring protective effects. Moreover, IFN alpha-2b treatment significantly reduces the pathogenicity of rhesus macaques against MPXV challenge (Figure 6). Regarding the differences in IFN-I administration timing between the mouse and rhesus macaque models, these were determined based on the distinct pharmacokinetics and clinical profiles of IFN-β and IFN-alpha-2b. In the CAST/EiJ mouse experiments, IFN-β (1 μg/mouse) was administered 3

hours prior to MPXV infection and again 2 days post-infection, guided by prior evidence of its short half-life and optimal therapeutic window for antiviral efficacy[33]. Conversely, in the rhesus macaque model, IFN-alpha-2b was administered 1 day before infection and 6 days post-infection, reflecting its longer half-life and clinical precedent of weekly dosing in humans, adapted here to assess prophylactic and therapeutic effects over a one-week interval. These timing differences account for species-specific responses and the IFN subtypes' pharmacokinetic properties, ensuring relevance to each model's infection dynamics. The result suggests that increasing the doses, frequency or combination of IFN-I with other anti-mpox drugs may completely antagonize MPXV challenge. Due to the limited number of rhesus macaques per group, only one animal in the IFN-alpha-2b treatment group achieved complete resolution of skin lesions, highlighting the need for additional nonhuman primate studies to further validate interferon's therapeutic efficacy and to optimize its timing and administration strategy. Moreover, the therapeutic effect of IFN-β and IFN alpha-2b treatment in mice and rhesus macaques in response to different MPXV clades also need to be further investigated. Collectively, these finding significantly advances our understanding of MPXV pathogenesis and offer potential avenues for mpox treatment.

Limitations of the study

There are several issues requiring further investigation. We observed splenomegaly in CAST/EiJ mice infected with the MPXV clade IIb strain, raising the need to explore whether similar effects occur in mice infected with other MPXV clades or orthopoxviruses.

Moreover, the recent surge in mpox cases caused by MPXV clade I in the Democratic Republic of Congo (DRC) and other African nations underscores the ongoing global public health threat posed by mpox. Consequently, future research should focus on the pathogenicity and critical mutations of the emerging MPXV clades, as well as evaluating the efficacy of Peg-IFN alpha-2b treatment against these new strains. Furthermore, the limited number of rhesus macaques in our Peg-IFN-alpha-2b experiments, coupled with the absence of histopathological analysis, necessitates additional nonhuman primate studies to fully elucidate interferon's therapeutic effects on disease onset and to optimize its timing and administration strategy.

STAR★METHODS

EXPERIMENTAL MODEL AND STUDY PARTICIPANT DETAILS

Ethics Statement

All procedures with infectious mpox virus (MPXV) were performed in registered select agent BSL-3 and ABSL-3 laboratories. The animals were group-housed in a ventilated cage system equipped with aerosol filter tops. All animal experiments were conducted following the guidelines approved by the Institutional Animal Care and Use Committee (IACUC) of the Institute of Laboratory Animal Science, Chinese Academy of Medical Sciences (approval No. XJ23002, XJ23005 and XJ24007). All procedures involving animals were conducted under anesthesia with 2% isoflurane (for mice) or 5mg/kg zoletil

50 (for monkeys) prior to sample collection to ensure their well-being, and every effort was made to minimize any potential animal suffering.

Low-passage stocks of MPXV clade IIb (MPXV-B.1-China-C-Tan-CQ01) were isolated from first imported mpox case of mainland China in 2022[29]. Viruses were cultivated in Vero cells and titrated via plaque assay as described previously[29]. All procedures were performed in a BSL-3 containment facility at the Institute of Laboratory Animal Science, Chinese Academy of Medical Sciences.

Mice

Four- to ten-week-old CAST/EiJ mice were obtained from the Institute of Laboratory Animal Science, Chinese Academy of Medical Sciences and were maintained in small ventilated microisolator cages. Mice were maintained in a pathogen-free, temperature-controlled, and 12 h light and dark cycle environment with the temperature maintained at 21–23 °C, relative humidity maintained at 50–60%, and free access to food and water at the animal biosafety level 3 (ABSL-3) containment facility, Institute of Laboratory Animal Science, Chinese Academy of Medical Sciences. Moreover, CAST/EiJ mice were anesthetized with 2% isopentane during dosing and MPXV IIb challenge.

Rhesus macaques

Six rhesus macaques aged 3 to 5 years were randomly divided into two groups (n=3/group) and treated twice with either Peg-IFN alpha-2b (60μg, Amoytop biotech, China) or saline control with 7-day intervals (1 days before and 6 days after MPXV infection) via subcutaneous (*s.c.*) route. On day 0, macaques were inoculated with 4×10^7 $TCID_{50}$ clade IIb MPXV (MPXV-B.1-China-C-Tan-CQ01) via the intravenous (*i.v.*) route and monitored

for 28 days for disease symptoms, including weight loss, body temperature, skin lesions, and viremia. To evaluate skin lesions in the rhesus macaque experiments, the operator was blinded to the group assignments prior to assessment, ensuring an unbiased analysis. The number of skin lesions was initially quantified by a single investigator and subsequently verified independently by a second observer. For the procedure, rhesus macaques were anesthetized with Zoletil-50, and lesion counts were performed within a biosafety cabinet.

Cells and viruses

Bone marrow-derived macrophages (BMDMs) were obtained by differentiating bone marrow progenitors from the bone marrow of CAST/EiJ and C57BL/6J mice. Cells were seeded on 6-well plates at a density of 2×10^6 cells per well and treated with 20 ng/ml M-CSF (Sino Biological) for 5 days in RPMI 1640 medium (Gibco). THP-1, and *STING*-knockout THP-1 cells were grown in RPMI 1640 medium (Gibco) and kindly provided by Prof. Conggang Zhang (Tsinghua University, Beijing, China). All media were supplemented with 10% heat-inactivated fetal bovine serum (FBS, Gibco), 2 mM L-glutamine, 100 units/ml penicillin and 100 units/ml streptomycin at 37 °C under an atmosphere with 5% CO_2. The cells were treated with DMXAA (MCE), H151 (MCE) and IFN-β (MCE), as indicated in the Figure. The cytotoxicity of the drugs used in this study was tested by performing a CCK-8 assay (Beyotime).

METHOD DETAILS

Quantification of viral DNA

Viral DNA from plasma and tissues was determined by quantitative PCR (qPCR) assay following a previously described method[30,43]. Briefly, viral DNA was extracted and

purified using a DNeasy Blood & Tissue Kit (QIAGEN). Quantitative PCR was carried out on an ABI 7500 Real-time PCR system (Applied Biosystems, Foster City, CA, USA) via TaqMan Gene Expression Master Mix (Applied Biosystems) using the following cycling protocol and primers: 50 °C for 2 min, 95 °C for 10 min, followed by 40 cycles at 95 °C for 15 s and 60 °C for 1 min. The sequences of the primers and probes targeted against the conserved region F3L[43] are shown in Table S1. The baseline values for viral DNA in plasma were determined based on the extraction and lysis volumes, with a cycle threshold (CT) value of the standard not exceeding 35.

Flow cytometry

The spleens of C57BL/6J and CAST/EiJ mice were minced and ground with a syringe plunger and passed through a 70 μm cell strainer. The cells were centrifuged at 400×g for 5 min at 4 °C, resuspended in PBS II (PBS and 1% BSA) at a concentration of 1×10^8 cells/ml, and 50 μl of the single-cell suspension was stained with the following antibodies: Brilliant Violet 510 conjugated anti-mouse CD3 (100234), PE/Cyanine7 conjugated anti-mouse CD19 (115520) from Biolegend, Alexa Fluor 700 conjugated anti-TCR beta (56-5961-82), APC-eFluor 780 conjugated anti-CD4 (47-0042-82), FITC conjugated anti-CD8a (11-0081-82), FITC conjugated anti-CD11c (17-0114-82), and PE conjugated anti-CD49b (Integrin alpha 2) (12-5971-82) from eBioscience. The staining was performed for 30 min at 4 °C. Data acquisition was carried out using a BD FACSAria II and analyzed using FlowJo v10 software.

$TCID_{50}$ of MPXV in mouse plasma and tissues

For the measurement of viral titers in the plasma and tissues of infected animals, $TCID_{50}$ (50% tissue culture infectious dose) assays were performed. After euthanasia, plasma and

tissue samples were collected, weighted, placed into pre-labeled cryovials, and stored at -80 °C. Prior to testing in the viral titer assays, tissue samples were thawed and placed in BMDM medium and were homogenized twice with 3-mm stainless steel beads for 20s at 75 HZ/s using tissue homogenizer (LUKA). Homogenates were spun down to remove debris, and supernatants were tested in the viral titer assays. Four-fold serial dilutions of plasma and tissue homogenates were made in BMDM medium. A serial dilution of plasma and tissue suspension were added to 90 to 100% confluent Vero E6 cells in triplicate wells. The plates for the samples were incubated at 37 °C for three days. After three days, wells were visually inspected for cytopathic effect (CPE). Non-infected wells were identified by a clear confluent cell layer. Infected cells demonstrated cell rounding. $TCID_{50}$ values per gram of tissue (or per ml of plasma) were calculated using the Reed-Muench method.

Histopathology and immunohistochemistry

Tissues from CAST/EiJ mice and rhesus macaques, were collected from each animal at the time of sacrifice at the end of the study period. These tissues were fixed in 4% paraformaldehyde and sectioned at 5 μm. Slides were baked for 30-60 min at 55 °C then deparaffinized in xylene and rehydrated through a serious of graded ethanol to distilled water, and stained with hematoxylin and eosin (H&E). For IHC, heat induced epitope retrieval (HIER) was performed using microwave oven in citrate buffer (Beijing ZSGB Biotechnology, ZLI-9065) followed by treatment with 3% hydrogen peroxide. After blocking in 1% normal goat serum (Beijing ZSGB Biotechnology, ZLI-9056), the sections were incubated with anti-CD68 antibody (Cell Signaling Technology, 97778), anti-Vaccinia antibody (Santa cruz, sc-58210) at 4 °C overnight. Subsequently, the sections were incubated with goat anti-mouse IgG secondary antibody (HRP) kits (Beijing ZSGB

Biotechnology, PV-9001) for 30 min, and visualized by 3,3'-diaminobenzidine tetrahydrochloride (DAB). The slices were counterstained with haematoxylin, dehydrated and mounted on a slide and viewed under an Olympus microscope. Images were taken with a 3D Histech (Hungary) Pannoramic MIDI microscope and viewed through CaseViewer 2.4. All pathological evaluations were performed by a pathologist with 10 years of histology experience and then confirmed by another pathologist.

Differential Gene Expression Analysis

Differential gene expression analysis was performed using DESeq2 (v1.44.0). RNA-seq count data from spleens of MPXV-infected and uninfected CAST/EiJ mice were processed following the standard DESeq2 workflow. Raw counts were normalized using DESeq2's median of ratios method to account for sequencing depth and RNA composition differences between samples. Differentially expressed genes (DEGs) were identified using the following criteria: absolute $\log_2$ fold change ($|\log_2 FC|$) ≥ 1 and adjusted *P*-value < 0.05 after Benjamini-Hochberg correction for multiple testing.

Functional Enrichment Analysis

Metascape enrichment analysis was conducted using the web interface (https://metascape.org/gp/index.html). Upregulated and downregulated genes were analyzed separately to identify distinct biological processes affected by MPXV infection. The top significantly enriched biological process terms for both upregulated and downregulated gene sets were selected based on adjusted *P*-values.

Western blotting

Cells were lysed in RIPA lysis buffer (Solarbio) supplemented with protease and phosphatase inhibitors. The supernatants were separated by SDS–PAGE after centrifugation and transferred to polyvinylidene difluoride membranes for immunoblot analyses using the following primary antibodies: anti-pSTING-S365 (Cell Signaling Technology, 72971, 1:500 dilution), anti-STING (Cell Signaling Technology, 50494, 1:1000 dilution), anti-pTBK1-S172 (Cell Signaling Technology, 5483, 1:1000 dilution), anti-TBK1 (Cell Signaling Technology, 3504, 1:1000 dilution), anti-pIRF3-S379 (Cell Signaling Technology, 79945, 1:1000 dilution), anti-IRF3 (Cell Signaling Technology, 4302, 1:1000 dilution), and HRP-conjugated anti-β-actin (Abcam, ab20272, 1:5000 dilution). After three washes, anti-rabbit HRP-conjugated antibodies were then applied, and the antigen–antibody complexes were visualized using chemiluminescence (ECL system, Immobilon Western Chemiluminescent HRP Substrate, Millipore). A PageRuler Western marker (Thermo) was used as a molecular weight standard.

Reverse transcription and quantitative RT–PCR

Total cellular RNA was prepared using a RNeasy Mini kit (QIAGEN, USA) according to the manufacturer's protocol. For cDNA synthesis, 0.5 μg of RNA was first digested with gDNA Eraser to remove contaminating DNA and then reverse transcribed using PrimeScript RT reagent kit mix with gDNA Eraser (RR047A, TaKaRa) in a 20 μl reaction volume. Then, 1 μl of cDNA was used as a template for quantitative PCR. The sequences of the primers used are shown in Table S1. The samples were denatured at 95 °C for 2 min, followed by 40 cycles of amplification (15 s at 94 °C for denaturation and 60 s at 60 °C for annealing and extension). Quantitative RT–PCR (qRT–PCR) was performed using Powerup SYBR Green Master Mix (A25742, Applied Biosystems) with an ABI 7500 Real-

time PCR system (Applied Biosystems, Foster City, CA, USA). Relative mRNA levels were normalized to those of β-actin and calculated using the $2^{-\Delta\Delta CT}$ method.

ELISA assay

BMDMs obtained from the bone marrow of C57BL/6J and CAST/EiJ mice were subsequently infected with MPXV at the indicated MOI. Cell cytosols were collected, and the concentration of 2' 3'-cGAMP was examined using ELISA kits according to the manufacturer's instructions (Cayman Chemical).

Immunofluorescence microscopy

BMDMs plated on glass coverslips were infected with MPXV (MOI=0.2). After fixation with 4% formaldehyde, the cells were permeabilized with 0.3% Triton X-100 in PBS for 15 min. After blocking with goat serum, the cells were incubated with anti-A29 (Sino Biological, 40891-M0032, 1:50 dilution) and anti-pSTING-S365 (Cell Signaling Technology, 62912, 1:100 dilution) or anti-pTBK1-S172 (Cell Signaling Technology, 5483, 1:100 dilution) antibodies overnight at 4 °C. The cells were subsequently washed three times with PBST solution and then incubated with FITC- or TRITC-conjugated goat anti-rabbit (or anti-mouse) IgG. The cells were then stained with DAPI after washing and imaged using a laser scanning confocal microscope (Zeiss LSM 800 Meta, built-in software ZEN2.3) with a 63× oil immersion lens. The intensity of pSTING or pTBK1 in cells was analyzed by ImageJ software.

QUANTIFICATION AND STATISTICAL ANALYSIS

Graphical representation and statistical analyses were performed using Prism 10.2.3 software (GraphPad software). The results are expressed as the means ± SEM. Differences between two independent samples were evaluated by two-tailed Student's *t*-tests. Differences between multiple samples were analyzed by one-way or two-way analysis of variance (ANOVA). Significance values were set as follows: ns (not significant), $P>0.05$; $^{*}P<0.05$; $^{**}P<0.01$; $^{***}P<0.001$.

Resource availability

Lead contact

Any further information or requests should be directed to, and will be fulfilled by, Dr. Jing Xue (xuejing@cnilas.org).

Materials availability

This study did not generate new unique reagents.

Data and code availability

The raw sequence data reported in this paper have been deposited in the Genome Sequence Archive in National Genomics Data Center, China National Center for Bioinformation / Beijing Institute of Genomics, Chinese Academy of Sciences under accession code of GSA: CRA023622. Accession numbers are listed in the key resources table. Any additional information required to reanalyze the data reported in this work paper is available from the Lead Contact upon request.

Acknowledgments

The authors thank Prof. Conggang Zhang (School of Pharmaceutical Sciences, Tsinghua University, Beijing, China) for kindly providing the THP-1 and THP-1 STING$^{-/-}$ cells. This work was funded by the National Key Research and Development Project of China (2022YFC2304100 to W.T., 2023YFC2309000 to J.X.), the National Natural Science Foundation of China (82241068 to J.X., 82222041 to J.X.) and the Beijing Natural Science Foundation (Z220018 to J.X.).

Author contributions: Conceived and designed the experiments: L.Z., W.T., and J.X.; performed the experiments: L.Z., Q.L., Y.H., B.H., D.Z., Z.C., J.M., N.L., J.L., J.Z., L.Y.Z, and T.C.; analyzed the data: L.Z., Q.L, Y.H., B.H, D.Z., and Z.C.; contributed reagents/materials/analysis tools: B.H., Q.W., J.L., W.T.; wrote and revised the article: L.Z., and J.X. All authors have read and approved the article.

Declaration of interests: The authors declare no competing interests.

Figure legends

Figure 1 Susceptibility of CAST/EiJ mice to MPXV clade IIb infection via *i.p.* and *i.n.* routes.

(A) Schematic diagram illustrating the experimental design for infection via the *i.p.* and *i.n.* routes in CAST/EiJ mice. A total of 48 CAST/EiJ mice were infected with MPXV clade IIb at 1.0×10^6 $TCID_{50}$ via the *i.p.* route (upper panel) or the *i.n.* route (lower panel). Mice were euthanized at 0, 4, 7, 11, 21, and 28 days post-infection (dpi, n=4 each time point), and peripheral blood and organs were collected.

(B, C) Examination and weight measurements were performed at 0, 4, 7, 11, 21, and 28 dpi in CAST/EiJ mice (n=4 per group) infected with MPXV clade IIb via the *i.p.* or *i.n.* route. The percentages of starting weights (B) and survival (C) are indicated.

(D) Plasma $\log_{10}$ viral DNA copies/ml (limit of detection: 1000 copies/ml) were quantified at 0, 4, 7, 11, 21, and 28 dpi.

(E) Heatmap displaying the $\log_{10}$ viral DNA levels (copies/μg DNA) in the heart, liver, spleen, lungs, kidneys, brain, intestines, stomach, and lymph nodes (inguinal lymph nodes).

(F, G) Viral titers in the plasma and tissues of MPXV clade IIb-infected CAST/EiJ mice via *i.p.* route at 4 dpi were titrated with $TCID_{50}$.

Differences between the groups were evaluated by a two-sided Student's *t*-tests (F) or two-way ANOVA (B, D, G) (ns, not significant; $*P < 0.01$; $***P < 0.001$). The dashed line indicates the limit of detection of the assay. The data are presented as the means ± SEM. Data in (D–G) are representative of two independent experiments.

See also Figure S1 and S2.

Figure 2 Splenic pathology and immune response in MPXV-infected CAST/EiJ mice.

(A) Representative images of spleens from CAST/EiJ mice infected with MPXV clade IIb via the *i.p.* and *i.n.* routes, harvested at 0, 4, 7, 11, 21, and 28 days post-infection (dpi). Scale bars: 1 cm.

(B) CAST mice were infected with MPXV clade IIb via the *i.p.* or *i.n.* route, and spleen weights were measured at 0, 4, 7, 11, 21, and 28 dpi. The percentage of spleen weight relative to body weight at the indicated dpi is shown.

(C) Histological analysis of spleen sections from CAST/EiJ mice challenged with or without MPXV clade IIb via the *i.p.* route. Tissue sections were stained with hematoxylin and eosin. Images were captured at 50× (upper panel) and 200× (lower panel). Arrows: black arrow indicates hyperplasia of the white pulp with prominent germinal centers, blue arrows indicate macrophage infiltration in the red pulp, and green arrows indicate extramedullary hematopoiesis in the red pulp.

(D, E) Immunohistochemistry (IHC) for macrophages and virus antigen in the spleen of CAST/EiJ mice challenged with or without MPXV clade IIb four days via the *i.p.* route. Images were captured at 200× (left panel) and 400× (right panel). Macrophages (brown in D) and MPXV antigen (brown in E) were performed with anti-CD68 and anti-Vaccinia virus antibodies. Nuclei were counterstained blue with hematoxylin. Arrows: red arrows indicate macrophages, black arrows indicate MPXV infection foci. The percentage of macrophages (right panel of D) and MPXV (right panel of E) in spleen was analyzed using ImageJ software.

(F) Analysis of the counts of B cells, T cells, NK cells and cDCs cells in the spleen of MPXV clade IIb -infected CAST/EiJ mice. Spleens were ground and adjusted to a final

volume of 1ml, and immune cell populations were analyzed via flow cytometry (FCM) assay.

(G) Proportion of $CD4^+$ T cells and $CD8^+$ T cells (left panel), and $CD4^+/CD8^+$ T ratio (right panel) in the spleen of MPXV clade IIb-infected CAST/EiJ mice were analyzed.

Differences between the groups were evaluated using two-way ANOVA (B, F, and left panel of G) or a two-sided unpaired Student's *t*-tests (right panel of D, E and G) (**$P < 0.01$; ***$P < 0.001$). The data are presented as the means ±SEM.

See also Figure S3 and S4.

Figure 3 The phosphorylation of STING, TBK1 and IRF3, and the transcription of IFN-β and its downstream genes were promoted in MPXV clade IIb infected BMDMs.

(A) Schematic diagram of the experimental design for MPXV clade IIb infection of BMDMs derived from CAST/EiJ and C57BL/6J mice. BMDMs were induced by M-CSF from the bone marrow of CAST/EiJ and C57BL/6J mice, and the cells were then infected with MPXV clade IIb.

(B) BMDMs obtained from C57BL/6J and CAST/EiJ mice were subsequently infected with MPXV clade IIb at the indicated MOI for 3 h, and the phosphorylation of STING, TBK1 and IRF3 in BMDMs was analyzed by immunoblotting. The pSTING/STING, pTBK1/TBK1 and pIRF3/IRF3 ratios were quantified through densitometry with ImageJ software, and the non-infected samples were assigned a value of 1.

(C) BMDMs obtained from C57BL/6J and CAST/EiJ mice were subsequently infected with MPXV clade IIb at the indicated MOI for 3 h, and the cGAMP levels in the cells were analyzed via ELISA assay.

(D) BMDMs obtained from C57BL/6J and CAST/EiJ mice were subsequently infected with MPXV clade IIb at the indicated MOI, and the mRNA level of IFN-β in BMDMs was quantified by qRT–PCR.

(E, G) BMDMs obtained from C57BL/6J and CAST/EiJ mice were infected with MPXV clade IIb (MOI=0.2). Twenty-four hours later, the cells were immunostained with anti-pSTING (red) (E) or anti-pTBK1 (red) (G) and anti-A29 (green) antibodies. Nuclei were stained with DAPI (blue), and images were obtained using a Zeiss LSM 800 Meta confocal microscope.

(F, H) The intensity of pSTING (F) or pTBK1 (H) in cells was analyzed by ImageJ software. The ratio of pSTING or pTBK1 distribution in 8 cells (n=8).

Differences between the groups were evaluated using two-way ANOVA (ns, not significant; $*P < 0.05$; $***P < 0.001$). The data are presented as the means ± SEM. At least two independent repeats were performed in all of the experiments.

See also Figure S5 and S6.

Figure 4 MPXV clade IIb promotes the transcription of IFN-β and its downstream genes via STING.

(A-E) BMDMs obtained from C57BL/6J and CAST/EiJ mice were infected with MPXV clade IIb (MOI=0.5). Then, the cells were treated with or without the STING inhibitor H151 (2 μM) for 3 h. The mRNA levels of IFN-β, CXCL10, ISG15, ISG56, and CCL5 in BMDMs were quantified by qRT–PCR.

(F) The efficiency of *STING*-knockout ($STING^{-/-}$) in THP-1 cells was determined using immunoblotting.

(G, H) WT and STING$^{-/-}$ THP-1 cells infected with MPXV clade IIb (MOI=0.1) for 24 h. The mRNA levels IFN-β (G) and its downstream genes CXCL10, ISG15 and ISG56 (H)were determined by qRT-PCR.

Differences between the groups were evaluated using two-way ANOVA (***$P < 0.001$). The data are presented as the means ± SEM. At least two independent replicates were performed in all experiments.

Figure 5 IFN-β significantly inhibits MPXV clade IIb replication in cells and in CAST/EiJ mice.

(A-C) BMDMs were infected with MPXV clade IIb (MOI=0.25). Then, the cells were treated with the indicated concentrations of the STING activator DMXAA (A), the STING inhibitor H151 (B), or the IFN-β protein (C) for 24 h. The number of MPXV genome copies in the cells was quantified via qRT–PCR.

(D) Schematic diagram of the experimental design showing the effect of IFN-β treatment on the replication of MPXV in CAST/EiJ mice. CAST/EiJ mice were administered with IFN-β (1 μg/mouse) or normal saline 3 h prior MPXV infection, 3 h post MPXV infection, 1 day post MPXV infection, and were infected with MPXV clade IIb (1.0×10^6 $TCID_{50}$) via the *i.p.* route, respectively (MPXV/Saline, MPXV/IFN-β -3h, MPXV/IFN-β +3h, MPXV/IFN-β +1d,). Subsequently, mice were re-administered IFN-β two days after the initial dose. On Day 4 post-infection, the mice were euthanized, and peripheral blood and tissues were collected.

(E) MPXV clade IIb-infected CAST/EiJ mice (n=5/group) were treated with or without IFN-β and weighed daily after MPXV infections. The percentage of the starting weight is indicated.

(F) IFN-β protein treatment significantly antagonizes splenomegaly in MPXV-induced CAST/EiJ mice. Splenomegaly is analyzed as the percentage of splenic weight relative to body weight.

(G) Plasma $\log_{10}$ viral DNA copies/ml were quantified using qRT–PCR.

(H) Log_{10} viral DNA in the heart, liver, spleen, lungs and kidneys was quantified using qRT–PCR.

Differences between the groups were evaluated one-way ANOVA (A-C, F, G) or two-way ANOVA (H, $*P < 0.05$; $**P < 0.01$; $***P < 0.001$). The data are presented as the means ± SEM. Data in (A–C) are representative of two independent experiments.

See also Figure S7.

Figure 6 IFN alpha-2b treatment significantly antagonize the pathogenicity of rhesus macaques against MPXV clade IIb challenge.

(A) Schematic illustrating experiment design in rhesus macaques.

(B, C) Rhesus macaques were monitored for body weight loss (B) and body temperature (C) for 0, 4, 7, 10, 14, 21, 28 days post MPXV infection.

(D) Poxvirus skin lesion counts were plotted and compared on days 0, 4, 7, 10, 14, 21, and 28 following MPXV challenge in the Peg-IFN alpha-2b or saline treated groups.

(E) Plasma $\log_{10}$ viral DNA copies/ml per animal were assessed on days 0, 4, 7, 10, 14, 21, and 28 following MPXV challenge in the Peg-IFN alpha-2b or saline treated groups.

Differences between the two groups were evaluated by a two-sided unpaired Student's *t*-tests (**P* < 0.05; ***P* < 0.01). The dashed line indicates the limit of detection of the assay. The data are presented as the means ± SEM.

See also Figure S8.

References

1. Lum, F.-M., Torres-Ruesta, A., Tay, M.Z., Lin, R.T.P., Lye, D.C., Rénia, L., and Ng, L.F.P. (2022). Monkeypox: disease epidemiology, host immunity and clinical interventions. Nature Reviews Immunology *22*, 597-613. 10.1038/s41577-022-00775-4.
2. Ophinni, Y., Frediansyah, A., Sirinam, S., Megawati, D., Stoian, A.M., Enitan, S.S., Akele, R.Y., Sah, R., Pongpirul, K., Abdeen, Z., et al. (2022). Monkeypox: Immune response, vaccination and preventive efforts. Narra J *2*. 10.52225/narra.v2i3.90.
3. Zandi, M., Shafaati, M., and Hosseini, F. (2023). Mechanisms of immune evasion of monkeypox virus. Frontiers in microbiology *14*. 10.3389/fmicb.2023.1106247.
4. Thornhill, J.P., Gandhi, M., and Orkin, C. (2024). Mpox: The Reemergence of an Old Disease and Inequities. Annual review of medicine *75*, 159-175. 10.1146/annurev-med-080122-030714.
5. WHO (2022). 2022-23 Mpox (Monkeypox) Outbreak: Global Trends. https://worldhealthorg.shinyapps.io/mpx_global/.
6. Aid, M., Sciacca, M., McMahan, K., Hope, D., Liu, J., Jacob-Dolan, C., Powers, O., Barrett, J., Wu, C., Mutoni, A., et al. (2023). Mpox infection protects against re-challenge in rhesus macaques. Cell *186*, 4652-4661 e4613. 10.1016/j.cell.2023.08.023.
7. Americo, J.L., Earl, P.L., and Moss, B. (2023). Virulence differences of mpox (monkeypox) virus clades I, IIa, and IIb.1 in a small animal model. Proceedings of the National Academy of Sciences *120*, e2220415120. 10.1073/pnas.2220415120.
8. Americo, J.L., Moss, B., and Earl, P.L. (2010). Identification of Wild-Derived Inbred Mouse Strains Highly Susceptible to Monkeypox Virus Infection for Use as Small Animal Models. J. Virol. *84*, 8172-8180. 10.1128/jvi.00621-10.
9. Earl, P.L., Americo, J.L., and Moss, B. (2012). Lethal Monkeypox Virus Infection of CAST/EiJ Mice Is Associated with a Deficient Gamma Interferon Response. J. Virol. *86*, 9105-9112. 10.1128/jvi.00162-12.
10. Americo, J.L., Sood, C.L., Cotter, C.A., Vogel, J.L., Kristie, T.M., Moss, B., and Earl, P.L. (2014). Susceptibility of the wild-derived inbred CAST/Ei mouse to infection by orthopoxviruses analyzed by live bioluminescence imaging. Virology *449*, 120-132. 10.1016/j.virol.2013.11.017.
11. Alakunle, E., Moens, U., Nchinda, G., and Okeke, M.I. (2020). Monkeypox Virus in Nigeria: Infection Biology, Epidemiology, and Evolution. Viruses *12*. 10.3390/v12111257.
12. Earl, P.L., Americo, J.L., and Moss, B. (2020). Natural killer cells expanded in vivo or ex vivo with IL-15 overcomes the inherent susceptibility of CAST mice to lethal infection with orthopoxviruses. PLoS pathogens *16*, e1008505. 10.1371/journal.ppat.1008505.
13. Warner, B.M., Klassen, L., Sloan, A., Deschambault, Y., Soule, G., Banadyga, L., Cao, J., Strong, J.E., Kobasa, D., and Safronetz, D. (2022). In vitro and in vivo efficacy of tecovirimat against a recently emerged 2022 monkeypox virus isolate. Science translational medicine *14*, eade7646. 10.1126/scitranslmed.ade7646.
14. Zuiani, A., Dulberger, C.L., De Silva, N.S., Marquette, M., Lu, Y.J., Palowitch, G.M., Dokic, A., Sanchez-Velazquez, R., Schlatterer, K., Sarkar, S., et al. (2024). A multivalent mRNA monkeypox virus vaccine (BNT166) protects mice and macaques from orthopoxvirus disease. Cell. 10.1016/j.cell.2024.01.017.

15. Jacob-Dolan, C., Ty, D., Hope, D., McMahan, K., Liu, J., Powers, O.C., Cotter, C.A., Sciacca, M., Wu, C., Borducchi, E., et al. (2024). Comparison of the immunogenicity and protective efficacy of ACAM2000, MVA, and vectored subunit vaccines for Mpox in rhesus macaques. Science translational medicine *16*, eadl4317. 10.1126/scitranslmed.adl4317.
16. Mucker, E.M., Freyn, A.W., Bixler, S.L., Cizmeci, D., Atyeo, C., Earl, P.L., Natarajan, H., Santos, G., Frey, T.R., Levin, R.H., et al. (2024). Comparison of protection against mpox following mRNA or modified vaccinia Ankara vaccination in nonhuman primates. Cell. 10.1016/j.cell.2024.08.043.
17. Goubau, D., Deddouche, S., and Reis e Sousa, C. (2013). Cytosolic Sensing of Viruses. Immunity *38*, 855-869. 10.1016/j.immuni.2013.05.007.
18. Sun, L., Wu, J., Du, F., Chen, X., and Chen, Z.J. (2012). Cyclic GMP-AMP Synthase Is a Cytosolic DNA Sensor That Activates the Type I Interferon Pathway. Science *339*, 786-791. 10.1126/science.1232458.
19. Wu, J., Sun, L., Chen, X., Du, F., Shi, H., Chen, C., and Chen, Z.J. (2012). Cyclic GMP-AMP Is an Endogenous Second Messenger in Innate Immune Signaling by Cytosolic DNA. Science *339*, 826-830. 10.1126/science.1229963.
20. Tanaka, Y., and Chen, Z.J. (2012). STING Specifies IRF3 Phosphorylation by TBK1 in the Cytosolic DNA Signaling Pathway. Science signal *5*.
21. Kato, K., Omura, H., Ishitani, R., and Nureki, O. (2017). Cyclic GMP-AMP as an Endogenous Second Messenger in Innate Immune Signaling by Cytosolic DNA. Annual review of biochemistry *86*, 541-566. 10.1146/annurev-biochem-061516-044813.
22. Hopfner, K.-P., and Hornung, V. (2020). Molecular mechanisms and cellular functions of cGAS–STING signalling. Nature Reviews Molecular Cell Biology *21*, 501-521. 10.1038/s41580-020-0244-x.
23. Dai, P., Wang, W., Cao, H., Avogadri, F., Dai, L., Drexler, I., Joyce, J.A., Li, X.D., Chen, Z., Merghoub, T., et al. (2014). Modified vaccinia virus Ankara triggers type I IFN production in murine conventional dendritic cells via a cGAS/STING-mediated cytosolic DNA-sensing pathway. PLoS pathogens *10*, e1003989. 10.1371/journal.ppat.1003989.
24. Cheng, W.-Y., He, X.-B., Jia, H.-J., Chen, G.-H., Jin, Q.-W., Long, Z.-L., and Jing, Z.-Z. (2018). The cGas–Sting Signaling Pathway Is Required for the Innate Immune Response Against Ectromelia Virus. Frontiers in immunology *9*. 10.3389/fimmu.2018.01297.
25. Georgana, I., Sumner, R.P., Towers, G.J., Maluquer de Motes, C., and Jung, J.U. (2018). Virulent Poxviruses Inhibit DNA Sensing by Preventing STING Activation. J. Virol. *92*. 10.1128/jvi.02145-17.
26. Eaglesham, J.B., Pan, Y., Kupper, T.S., and Kranzusch, P.J. (2019). Viral and metazoan poxins are cGAMP-specific nucleases that restrict cGAS-STING signalling. Nature *566*, 259-263. 10.1038/s41586-019-0928-6.
27. Parekh, N.J., Krouse, T.E., Reider, I.E., Hobbs, R.P., Ward, B.M., and Norbury, C.C. (2019). Type I interferon-dependent CCL4 is induced by a cGAS/STING pathway that bypasses viral inhibition and protects infected tissue, independent of viral burden. PLoS pathogens *15*, e1007778. 10.1371/journal.ppat.1007778.
28. Johnston, S.C., Lin, K.L., Connor, J.H., Ruthel, G., Goff, A., and Hensley, L.E. (2012). In vitro inhibition of monkeypox virus production and spread by Interferon-beta. Virol J *9*, 5. 10.1186/1743-422X-9-5.
29. Huang, B., Zhao, H., Song, J., Zhao, L., Deng, Y., Wang, W., Lu, R., Wang, W., Ren, J., Ye, F., et al. (2022). Isolation and Characterization of Monkeypox Virus from the First Case of Monkeypox - Chongqing Municipality, China, 2022. China CDC weekly *4*, 1019-1024. 10.46234/ccdcw2022.206.
30. Zhao, H., Wang, W., Zhao, L., Ye, S., Song, J., Lu, R., Zong, H., Wu, C., Huang, W., Huang, B., et al. (2022). The First Imported Case of Monkeypox in the Mainland of China - Chongqing Municipality, China, September 16, 2022. China CDC weekly *4*, 853-854. 10.46234/ccdcw2022.175.
31. Mazzotta, V., Nozza, S., Lanini, S., Moschese, D., Tavelli, A., Rossotti, R., Fusco, F.M., Biasioli, L., Matusali, G., Raccagni, A.R., et al. (2024). Clinical and laboratory predictors of mpox severity and duration: an Italian multicentre cohort study (mpox-Icona). eBioMedicine *107*. 10.1016/j.ebiom.2024.105289.
32. Kmiec, D., and Kirchhoff, F. (2022). Monkeypox: A New Threat? International journal of molecular sciences *23*. 10.3390/ijms23147866.
33. Karki, R., Lee, S., Mall, R., Pandian, N., Wang, Y., Sharma, B.R., Malireddi, R.S., Yang, D., Trifkovic, S., Steele, J.A., et al. (2022). ZBP1-dependent inflammatory cell death, PANoptosis, and cytokine storm disrupt IFN therapeutic efficacy during coronavirus infection. Science immunology *7*, eabo6294.

10.1126/sciimmunol.abo6294.
34. Chiuppesi, F., Zaia, J.A., Gutierrez-Franco, M.A., Ortega-Francisco, S., Ly, M., Kha, M., Kim, T., Dempsey, S., Kar, S., Grifoni, A., et al. (2024). Synthetic modified vaccinia Ankara vaccines confer cross-reactive and protective immunity against mpox virus. Commun Med (Lond) *4*, 19. 10.1038/s43856-024-00443-9.
35. Tang, D., Liu, X., Lu, J., Fan, H., Xu, X., Sun, K., Wang, R., Li, C., Dan, D., Du, H., et al. (2023). Recombinant proteins A29L, M1R, A35R, and B6R vaccination protects mice from mpox virus challenge. Frontiers in immunology *14*, 1203410. 10.3389/fimmu.2023.1203410.
36. Li, H., Huang, Q.-Z., Zhang, H., Liu, Z.-X., Chen, X.-H., Ye, L.-L., and Luo, Y. (2023). The land-scape of immune response to monkeypox virus. eBioMedicine *87*, 104424. 10.1016/j.ebiom.2022.104424.
37. Viallard, J.F., Parrens, M., Blanco, P., Moreau, J.F., Oksenhendler, E., and Fieschi, C. (2024). Influence of Splenomegaly and Splenectomy on the Immune Cell Profile of Patients with Common Variable Immunodeficiency Disease. J Clin Immunol *44*, 46. 10.1007/s10875-023-01648-8.
38. Jiao, P., Ma, J., Zhao, Y., Jia, X., Zhang, H., Fan, W., Jia, X., Bai, X., Zhao, Y., Lu, Y., et al. (2024). The nuclear localization signal of monkeypox virus protein P2 orthologue is critical for inhibition of IRF3-mediated innate immunity. Emerging microbes & infections *13*. 10.1080/22221751.2024.2372344.
39. Arndt, W.D., Cotsmire, S., Trainor, K., Harrington, H., Hauns, K., Kibler, K.V., Huynh, T.P., Jacobs, B.L., and McFadden, G. (2015). Evasion of the Innate Immune Type I Interferon System by Monkeypox Virus. J. Virol. *89*, 10489-10499. 10.1128/jvi.00304-15.
40. Zhang, L., Wei, X., Wang, Z., Liu, P., Hou, Y., Xu, Y., Su, H., Koci, M.D., Yin, H., and Zhang, C. (2023). NF-κB activation enhances STING signaling by altering microtubule-mediated STING trafficking. Cell reports *42*. 10.1016/j.celrep.2023.112185.
41. El-Jesr, M., Teir, M., and Maluquer de Motes, C. (2020). Vaccinia Virus Activation and Antagonism of Cytosolic DNA Sensing. Frontiers in immunology *11*, 568412. 10.3389/fimmu.2020.568412.
42. Hervas-Stubbs, S., Perez-Gracia, J.L., Rouzaut, A., Sanmamed, M.F., Le Bon, A., and Melero, I. (2011). Direct effects of type I interferons on cells of the immune system. Clinical cancer research : an official journal of the American Association for Cancer Research *17*, 2619-2627. 10.1158/1078-0432.CCR-10-1114.
43. Wei, Q., Huang, B., Huang, W., Song, J., Mei, L., Zhao, L., Yin, J., Zhang, J., Wang, W., Ye, F., et al. (2022). The first strain of monkeypox isolated in the Chinese Mainland and preserved at the National Pathogen Resource Center of China. Infectious Medicine *1*, 288-291. 10.1016/j.imj.2022.11.003.

CellPress

KEY RESOURCE TABLE

REAGENT or RESOURCE	SOURCE	IDENTIFIER
Antibodies		
Phospho-STING (Ser365) (D8F4W) Rabbit mAb	Cell Signaling Technology	Cat# 72971, RRID:AB_2799831
Phospho-STING (Ser365) (D1C4T) Rabbit mAb	Cell Signaling Technology	Cat# 62912, RRID:AB_2799635
STING (D1V5L) Rabbit mAb (Rodent Preferred)	Cell Signaling Technology	Cat# 50494, RRID:AB_2799375
Phospho-TBK1/NAK (Ser172) (D52C2) XP Rabbit monoclonal Antibody	Cell Signaling Technology	Cat# 5483, RRID:AB_10693472
TBK1/NAK (D1B4) XP (tm) Rabbit mAb	Cell Signaling Technology	Cat# 3504, RRID:AB_2255663
Phospho-IRF-3 (Ser379) (E6F7Q) Rabbit mAb	Cell Signaling Technology	Cat# 79945, RRID:AB_2799943
IRF-3 (D83B9) Rabbit mAb	Cell Signaling Technology	Cat# 4302, RRID:AB_1904036
Monkeypox Virus (MPXV) A5L Antibody, Mouse MAb	SinoBiological	Cat# 40905-M0075
Monkeypox Virus (MPXV) A29 Antibody, Mouse MAb	SinoBiological	Cat# 40891-M0032
Mouse Anti-beta Actin - Loading Control Monoclonal Antibody	Abcam	Cat# ab20272, RRID:AB_445482
CD68 (E3O7V) Rabbit mAb	Cell Signaling Technology	Cat# 97778, RRID:AB_2928056
Vaccinia Virus antibody (8115)	Santa Cruz Biotechnology	Cat# sc-58210, RRID:AB_632582
Goat Anti-Rabbit IgG H&L (HRP)	Abcam	Cat# ab205718, RRID:AB_2819160
Goat Anti-Mouse IgG H&L (HRP)	Abcam	Cat# ab205719, RRID:AB_2755049
Rhodamine (TRITC) - Conjugated Goat anti-Rabbit IgG (H+L)	ZSGB-Bio	Cat# ZF-0316, RRID:AB_2728778
FITC labeled goat anti-mouse IgG	ZSGB-Bio	Cat# ZF-0312, RRID:AB_2716306
Brilliant Violet 510(TM) anti-mouse CD3	Bioledend	Cat# 100234, RRID:AB_2562555
PE/Cyanine7 anti-mouse CD19	Bioledend	Cat# 115520, RRID:AB_313655
TCR beta Monoclonal Antibody (H57-597), Alexa Fluor™ 700, eBioscience	Thermo Fisher Scientific	Cat# 56-5961-82, RRID:AB_2802349
CD4 Monoclonal Antibody (RM4-5), APC-eFluor™ 780, eBioscience	Thermo Fisher Scientific	Cat# 47-0042-82, RRID:AB_1272183
CD8a Monoclonal Antibody (53-6.7), FITC, eBioscience	Thermo Fisher Scientific	Cat# 11-0081-82, RRID:AB_464915
CD11c Monoclonal Antibody (N418), APC, eBioscience	Thermo Fisher Scientific	Cat# 17-0114-82, RRID:AB_469346
CD49b (Integrin alpha 2) Monoclonal Antibody (DX5), PE, eBioscience	Thermo Fisher Scientific	Cat# 12-5971-82, RRID:AB_466073
Bacterial and virus strains		

Mpox virus clade IIb	Huang et al[29]	MPXV-B.1-China-C-Tan-CQ01
Biological samples		
Bone marrow-derived macrophages	This paper	N/A
Chemicals, peptides, and recombinant proteins		
M-CSF	SinoBiological	Cat# 51112-M08H
DMAXX	MedChemExpress	Cat# HY-10964
H151	MedChemExpress	Cat# HY-112693
IFN-beta	MedChemExpress	Cat# HY-P73130
Peg-IFN alpha-2b	Amoytop biotech	Cat# NMPA S20160001
Critical commercial assays		
CCK-8 assay	Beyotime	Cat# C0038
2'3'-cGAMP ELISA Kit	Cayman Chemical	Cat# 501700
cOmplete Protease Inhibitor Cocktail	Roche Biochemicals	Cat# 4693132001
PhosSTOP	Roche Biochemicals	Cat# 4906837001
Deposited data		
Raw and analyzed data (RNA-seq)	This paper	GSA: CRA023622
Experimental models: Cell lines		
THP-1 cells	Conggang Zhang (Tsinghua University, Beijing, China)	N/A
STING-knockout THP-1 cells	Conggang Zhang (Tsinghua University, Beijing, China)	N/A
Experimental models: Organisms/strains		
CAST/EiJ mice	Institute of Laboratory Animal Science, Chinese Academy of Medical Sciences	N/A
C57BL/6J mice	Clarles River	Cat#: 219
Rhesus Macaques	Dr. Xue's Lab in ILAS, CAMS	N/A
Oligonucleotides		
Primers for qRT-PCR, see Table S1	This paper	N/A
Software and algorithms		
GraphPad Prism	https://www.graphpad.com/	Version 10.2.3
Adobe Photoshop	https://www.adobe.com/products/photoshop.html	Adobe 21.2.0
FlowJo	https://www.flowjo.com/solutions/flowjo	FlowJo 10.4
FIJI ImageJ	https://fiji.sc	RRID: SCR_002285

Figure 1

Click here to access/download;Figure;Figure 1.tif

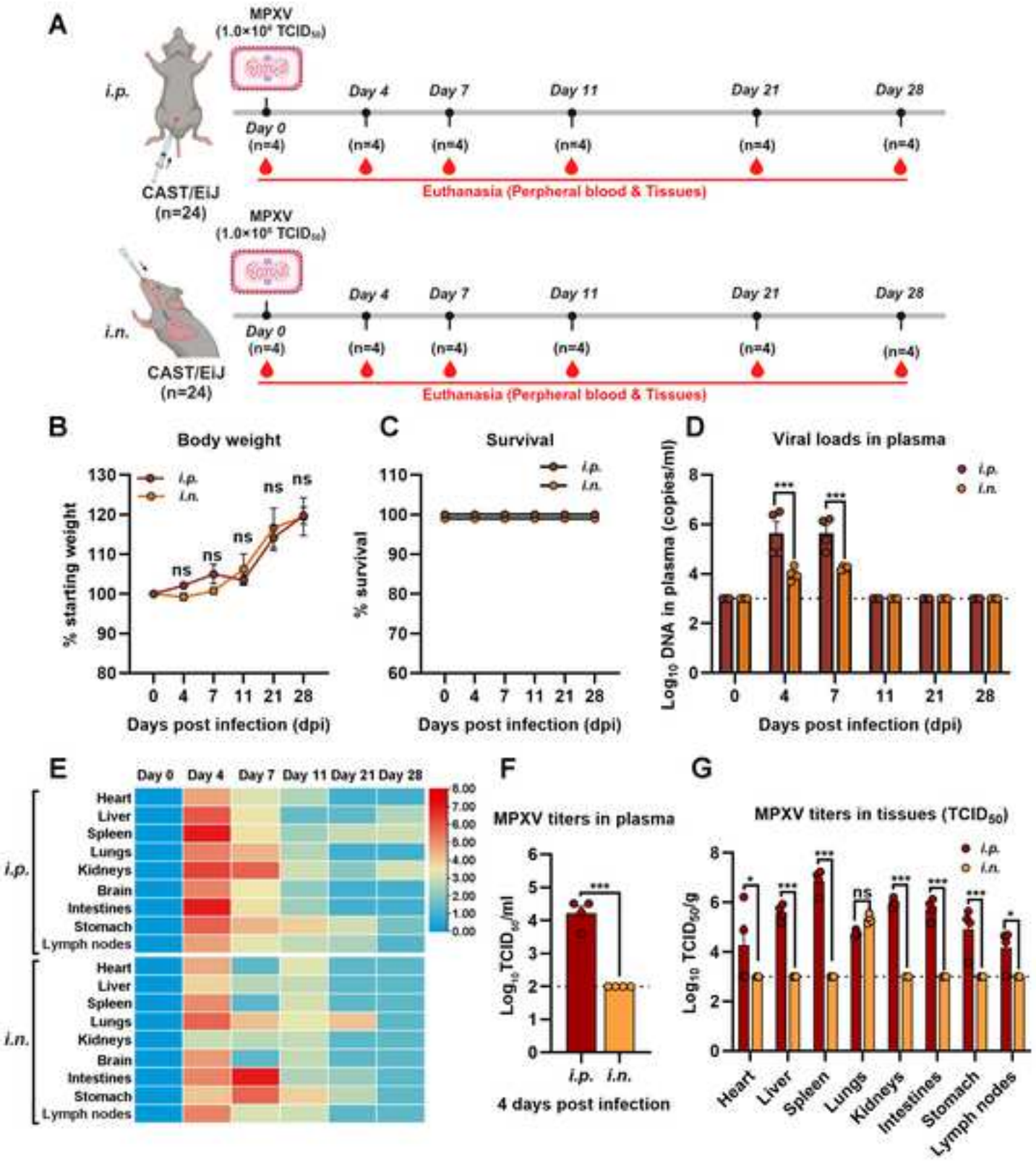

Figure 2

Click here to access/download;Figure;Figure 2.tif

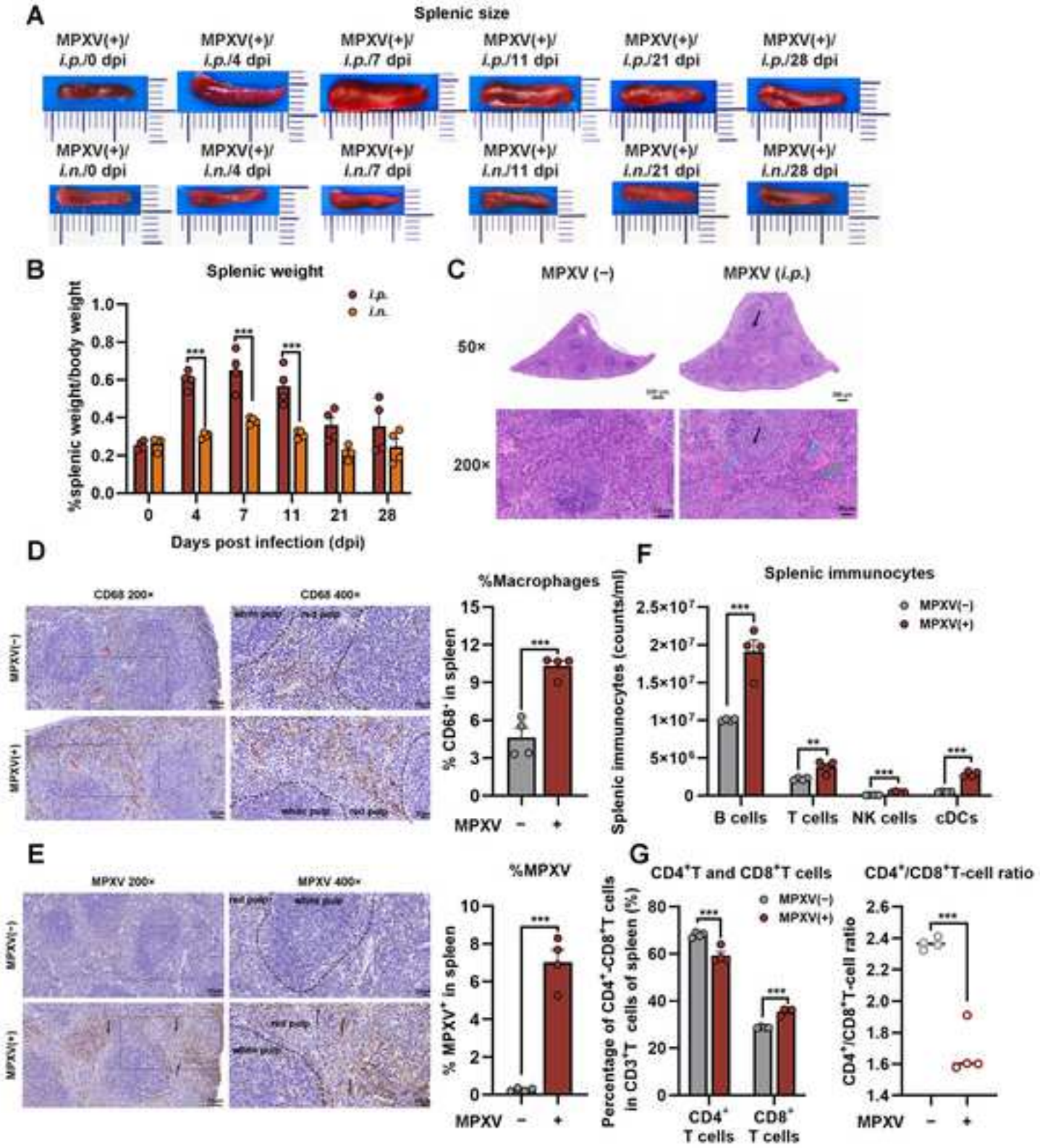

Figure 3

Click here to access/download;Figure;Figure 3.tif

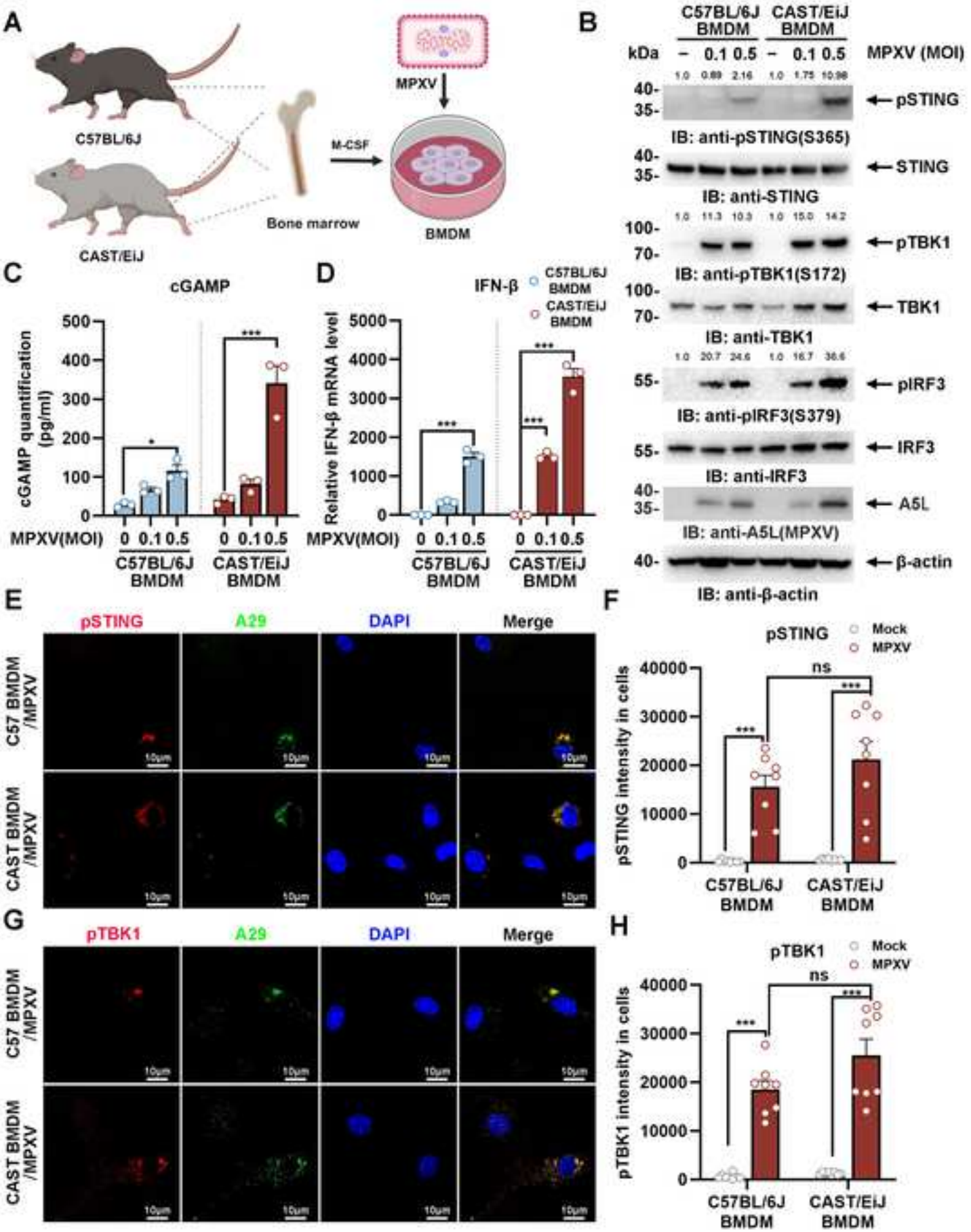

Figure 4

Click here to access/download;Figure;Figure 4.tif

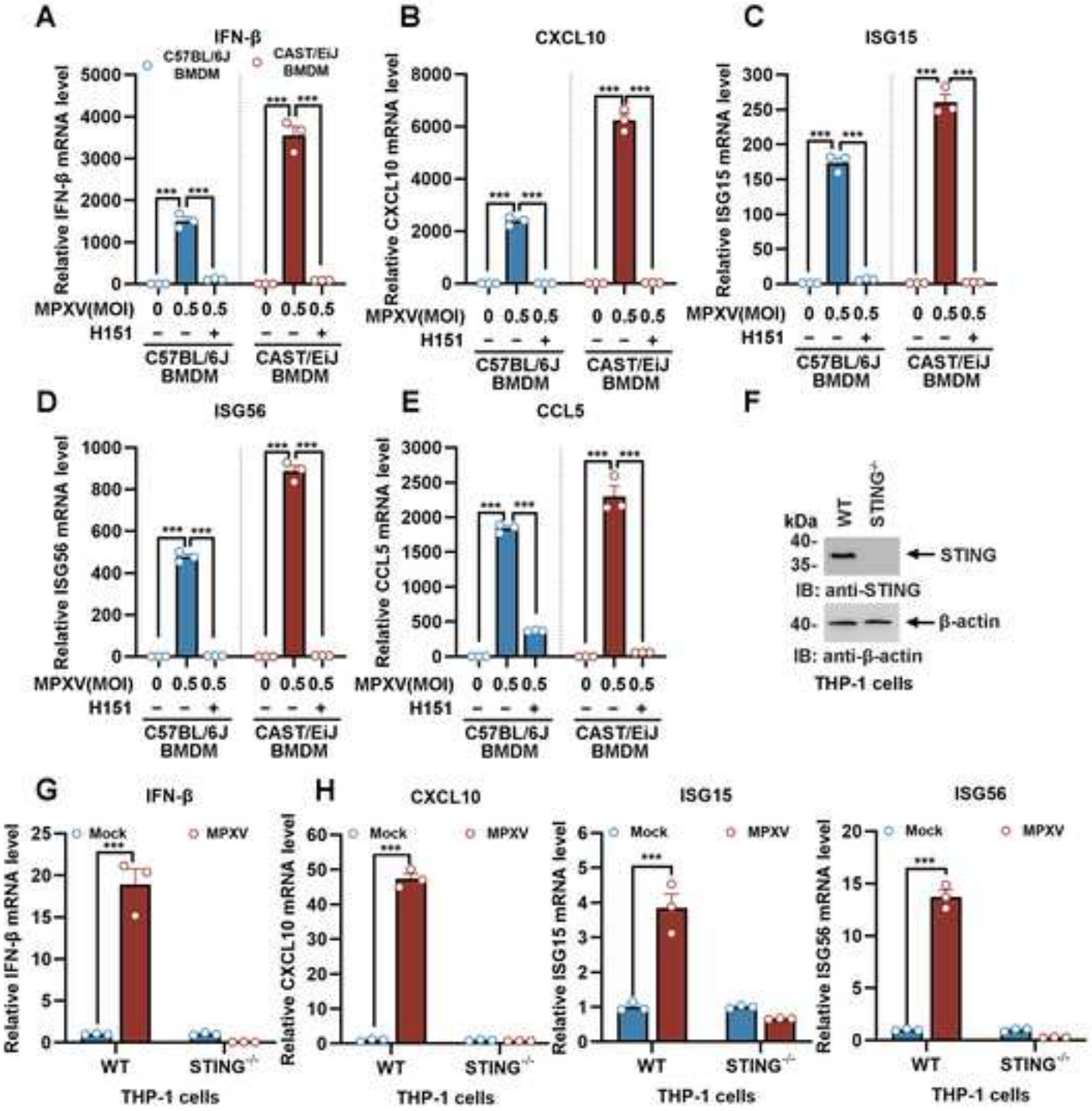

Figure 5

Click here to access/download;Figure;Figure 5.tif

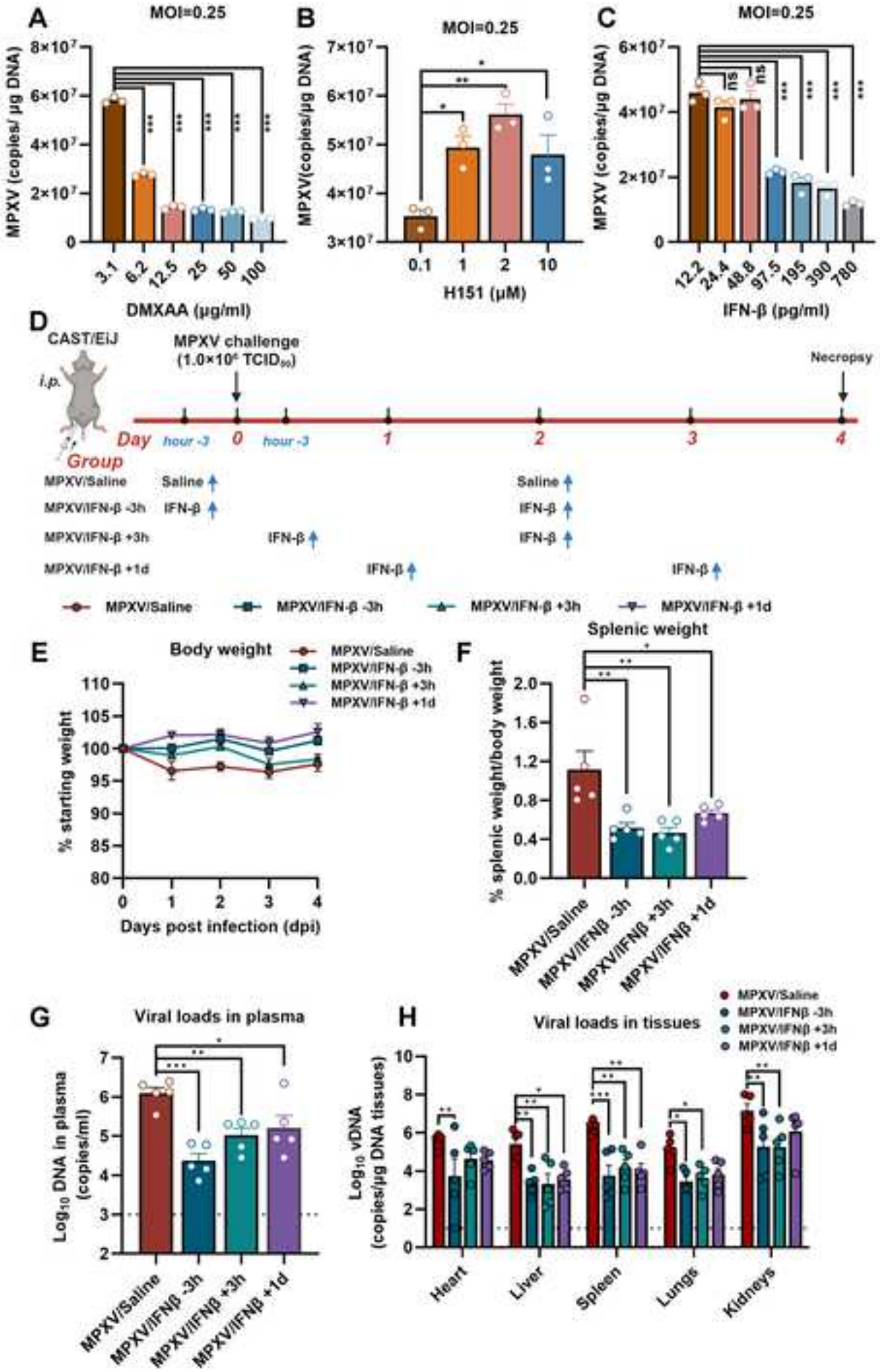

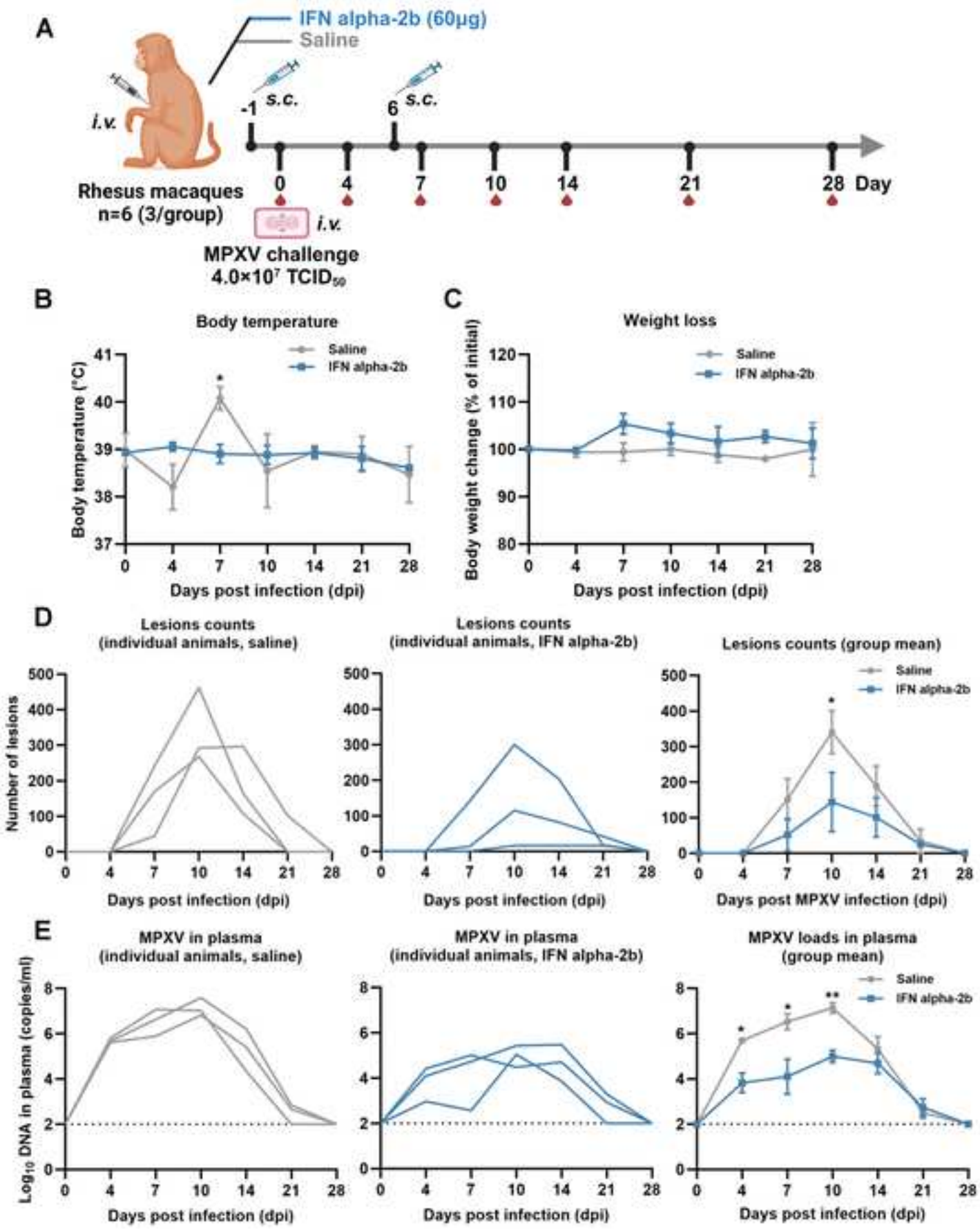
A
IFN alpha-2b (60μg)
Saline
i.v.
s.c.
-1
6
s.c.
0
4
7
10
14
21
28
Day
Rhesus macaques
n=6 (3/group)
i.v.
MPXV challenge
4.0×10⁷ TCID50
B
Body temperature
Saline
IFN alpha-2b
Body temperature (°C)
Days post infection (dpi)
C
Weight loss
Saline
IFN alpha-2b
Body weight change (% of initial)
Days post infection (dpi)
D
Lesions counts
(individual animals, saline)
Lesions counts
(individual animals, IFN alpha-2b)
Lesions counts (group mean)
Saline
IFN alpha-2b
Number of lesions
Days post infection (dpi)
Days post MPXV infection (dpi)
E
MPXV in plasma
(individual animals, saline)
MPXV in plasma
(individual animals, IFN alpha-2b)
MPXV loads in plasma
(group mean)
Saline
IFN alpha-2b
Log10 DNA in plasma (copies/ml)
Days post infection (dpi)

Supplemental Information

MPXV infection activates cGAS-STING signaling and IFN-I treatment reduces pathogenicity of mpox in CAST/EiJ mice and rhesus macaques

Lin Zhu[1,4], Qi Liu[1,4], Yongzhi Hou[1,4], Baoying Huang[2,4], Dong Zhang[1], Zhe Cong[1], Jianrong Ma[1], Na Li[1], Jiahan Lu[1], Jingjing Zhang[1], Lingyan Zhang[1], Ting Chen[1], Qiang Wei[1,3], Jiangning Liu[1], Wenjie Tan[2,*], and Jing Xue[1,3,5,*]

[1]NHC Key Laboratory of Human Disease Comparative Medicine, Beijing Key Laboratory for Animal Models of Emerging and Remerging Infectious Diseases, Institute of Laboratory Animal Science, Chinese Academy of Medical Sciences and Peking Union Medical College, Beijing, 100021, China

[2]NHC Key Laboratory of Biosafety, National Key Laboratory of Intelligent Tracking and Forecasting for Infectious Diseases, National Institute for Viral Disease Control and Prevention, Chinese Center for Disease Control and Prevention, Beijing, 102206, China

[3]State Key Laboratory of Respiratory Health and Multimorbidity, Key Laboratory of Pathogen Infection Prevention and Control (Peking Union Medical College), Ministry of Education, Institute of Laboratory Animal Science, Chinese Academy of Medical Sciences, Beijing, 100021, China

[4]These authors contributed equally

[5]Lead contact

[*]Correspondence to: Jing Xue (xuejing@cnilas.org), and Wenjie Tan (tanwj@ivdc.chinacdc.cn)

This PDF file includes:

Figure S1 to S8 and Table S1

A

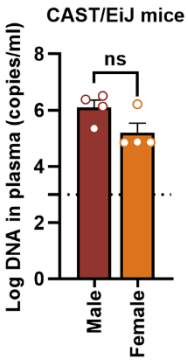

B

i.p. infection route	Day 4				Day 7				Day 11			
Tissues	*i.p.* 4-1	*i.p.* 4-2	*i.p.* 4-3	*i.p.* 4-4	*i.p.* 7-1	*i.p.* 7-2	*i.p.* 7-3	*i.p.* 7-4	*i.p.* 11-1	*i.p.* 11-2	*i.p.* 11-3	*i.p.* 11-4
Heart	4.94	5.30	3.08	5.23	3.24	3.60	2.76	3.10	3.27	3.29	3.52	1.92
Liver	6.27	6.29	5.01	6.21	3.47	4.00	2.99	3.93	1.30	1.63	1.72	1.14
Spleen	7.13	7.86	6.03	6.98	3.54	3.60	3.95	3.34	2.59	2.37	1.74	2.69
Lungs	5.37	5.56	4.40	5.77	4.60	4.38	4.16	4.44	2.85	1.95	3.06	2.50
Kidneys	6.90	6.92	5.01	6.47	6.59	6.40	5.91	4.26	3.40	3.00	3.27	2.48
Brain	5.71	5.75	4.82	4.68	3.62	4.63	3.70	2.14	2.10	2.17	2.17	2.14
Intestines	6.78	8.15	5.30	7.67	3.91	3.35	3.75	3.70	1.99	3.96	1.11	2.20
Stomach	5.13	6.14	5.22	6.67	3.99	3.79	5.22	4.44	3.24	5.77	2.78	3.50
Lymph nodes	5.25	5.03	3.65	5.02	3.42	4.29	3.19	2.35	3.63	3.53	3.58	2.13

C

i.n. infection route	Day 4				Day 7				Day 11			
Tissues	*i.n.* 4-1	*i.n.* 4-2	*i.n.* 4-3	*i.n.* 4-4	*i.n.* 7-1	*i.n.* 7-2	*i.n.* 7-3	*i.n.* 7-4	*i.n.* 11-1	*i.n.* 11-2	*i.n.* 11-3	*i.n.* 11-4
Heart	3.45	4.14	2.57	3.67	2.75	2.22	2.73	2.07	1.63	2.43	1.69	2.16
Liver	2.85	3.50	2.24	2.67	1.74	1.98	1.32	1.28	1.50	2.14	1.91	1.80
Spleen	3.27	4.73	3.28	3.77	2.31	1.65	1.48	1.75	1.75	2.32	1.95	2.34
Lungs	3.57	2.91	6.34	5.87	3.96	3.52	3.62	3.57	1.76	3.24	2.57	3.12
Kidneys	2.40	1.24	2.94	2.16	1.37	1.67	2.76	1.45	2.14	1.77	2.03	1.68
Brain	3.29	3.93	3.55	3.12	1.84	2.20	2.40	2.07	2.11	1.70	1.90	1.85
Intestines	3.89	4.31	3.38	4.47	5.21	5.48	5.56	5.43	1.92	1.47	1.80	2.11
Stomach	3.38	2.05	3.70	3.16	4.76	2.90	5.12	4.42	2.42	2.91	1.81	2.19
Lymph nodes	4.52	3.03	4.10	3.22	4.43	2.17	4.06	3.16	2.01	2.27	2.56	1.83

D

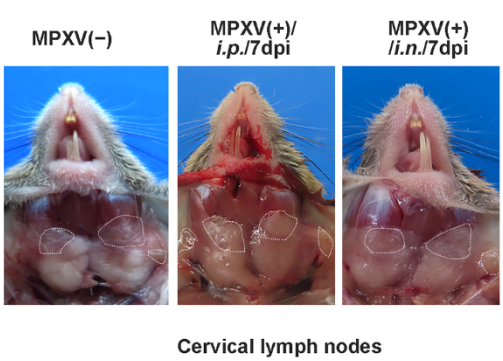

Figure S1 Viral loads and lymphadenopathy of MPXV clade IIb-infected CAST/EiJ mice. Related to Figure 1.

(A)CAST/EiJ mice infected with MPXV clade IIb via the *intraperitoneal* (*i.p.*) route were placed together at 4 and 7 days post-infection (dpi) to compare the viral loads in the plasma of male and female mice. Statistical analysis was conducted using a two-sided unpaired Student's *t*-tests. The data are presented as the means ± SEM (ns, not significant).

(B, C) Viral loads in the heart, liver, spleen, lungs, kidneys, brain, intestines, stomach, and lymph nodes at 4, 7, and 11 dpi following MPXV clade IIb infection via the *i.p.* (B) or intranasal (*i.n.*) (C) route in CAST/EiJ mice.

(D) Cervical lymphadenopathy occurred at 7 dpi in MPXV clade IIb-infected CAST/EiJ mice, represented by dotted outlines around the cervical lymph nodes.

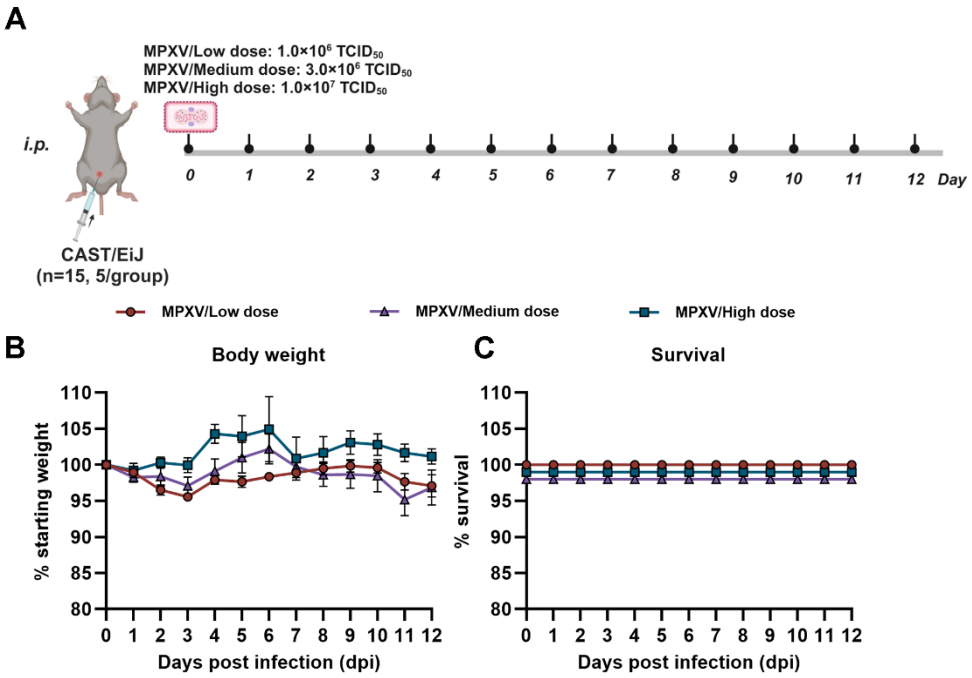

Figure S2 Higher concentration (1×10^7 $TCID_{50}$) of MPXV clade IIb-infected CAST/EiJ mice showed no significant changes in their body weight and survival. Related to Figure 1.
(A) Schematic diagram illustrating the experimental design for MPXV infection in CAST/EiJ mice via the *i.p.* route. The three groups of CAST/EiJ mice were infected with 1×10^6 $TCID_{50}$, 3×10^6 $TCID_{50}$, and 1×10^7 $TCID_{50}$ of MPXV clade IIb, respectively.
(B, C) CAST/EiJ mice infected with MPXV clade IIb via the *i.p.* route was monitored for body weight and survival. Percentages of starting body weight (B) and survival (C) are presented. The data are presented as means ±SEM.

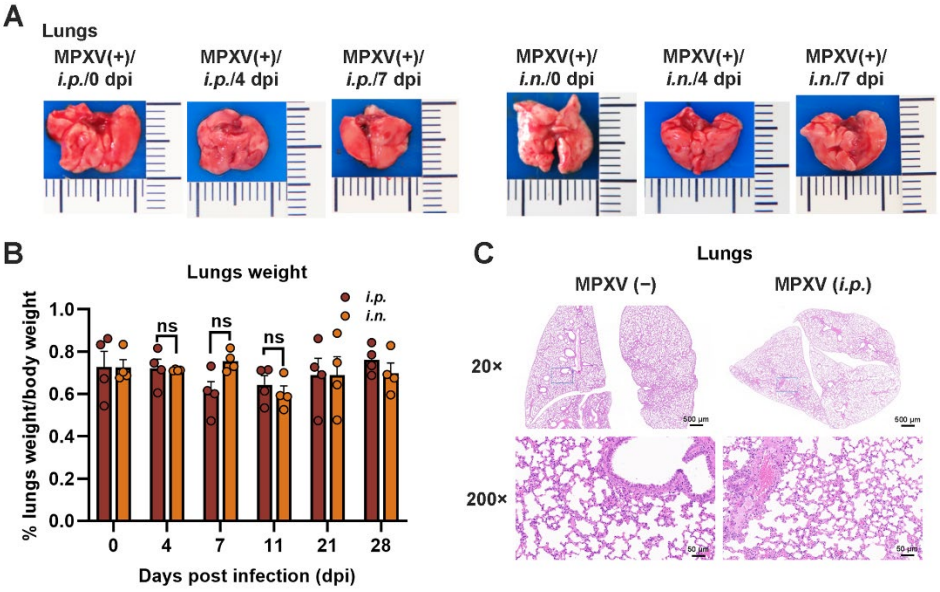

Figure S3 MPXV clade IIb-infected CAST/EiJ mice showed no significant changes in lung weight, gross pathology and histopathology, Related to Figure 2.

(A) Gross pathology of lungs in MPXV clade IIb-infected CAST/EiJ mice were monitored via the *i.p.* or *i.n.* routes at the indicated dpi.

(B) CAST mice were infected with MPXV clade IIb via the *i.p.* or *i.n.* routes (n=4 for *i.p.*, n=3 for *i.n.*), and lung weights were measured at 0, 4, 7, 11, 21, and 28 dpi. The lung weight as a percentage of body weight at the indicated dpi is shown. Differences between the groups were evaluated using two-way ANOVA (ns, not significant). The data are presented as means ±SEM.

(C) Histopathology of lungs in CAST/EiJ mice infected with MPXV clade IIb via the *i.p.* route. Representative images of lung tissues in CAST/EiJ mice were shown on day 7 after MPXV infection. Tissue sections were stained with hematoxylin and eosin. Images were captured at 20× (upper panel) and 200× (lower panel).

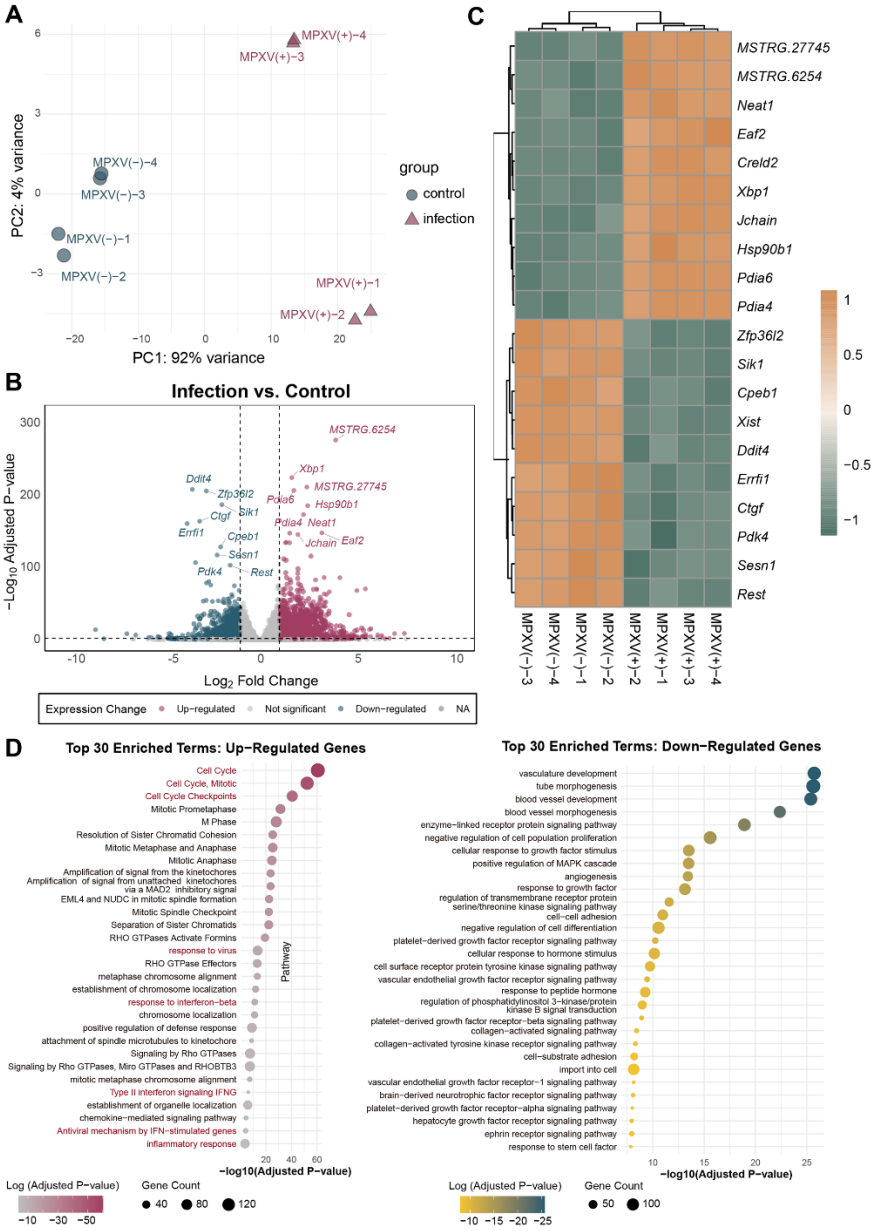

Figure S4 Transcriptomic signatures in spleen of MPXV-infected CAST/EiJ mice. Related to Figure 2.
(A) Principal component analysis (PCA) of splenic transcriptomic profiles from MPXV-infected [MPXV(+)] and uninfected [MPXV(-)] CAST/EiJ mice at 4 days post-infection. Each dot represents an individual animal.
(B) Volcano plot displaying differentially expressed genes in spleens of MPXV-infected CAST/EiJ mice. Significantly differentially expressed genes ($|\log_2 FC| \geq 1$ and adjusted $P<0.05$) are highlighted, with red dots indicating significant upregulation and green dots representing significant downregulation. Non-significant genes are shown in grey.
(C) Heatmap displaying the top differentially expressed genes following MPXV infection. Columns represent individual mice and rows correspond to individual genes. Color intensity reflects normalized gene expression values derived from DESeq2 analysis.
(D) Dot plots illustrating the 30 biological process terms enriched in upregulated (left panel) and downregulated (right panel) genes following MPXV infection, analyzed using Metascape. Dot size corresponds to the number of genes associated with each term, while color intensity represents statistical significance [$-\log_{10}$ (adjusted P-value)].

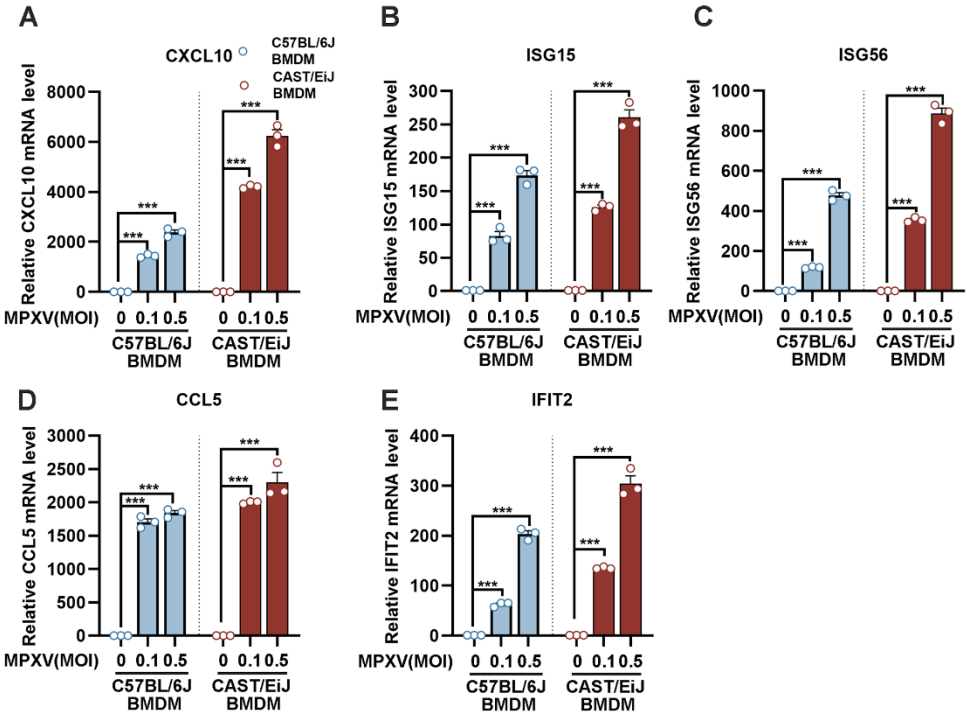

Figure S5 Transcriptional upregulation of CXCL10, ISG15, ISG56, CCL5 and IFIT2 in BMDMs from C57BL/6J and CAST/EiJ mice following MPXV clade IIb infection, Related to Figure 3.
(A-E) BMDMs derived from C57BL/6J and CAST/EiJ mice were infected with MPXV clade IIb at the indicated MOI, and the mRNA expression levels of CXCL10 (A), ISG15 (B), ISG56 (C), CCL5 (D) and IFIT2 (E) were quantified by qRT–PCR. Differences between the groups were evaluated using two-way ANOVA (***$P < 0.001$). The data are presented as the means ± SEM.

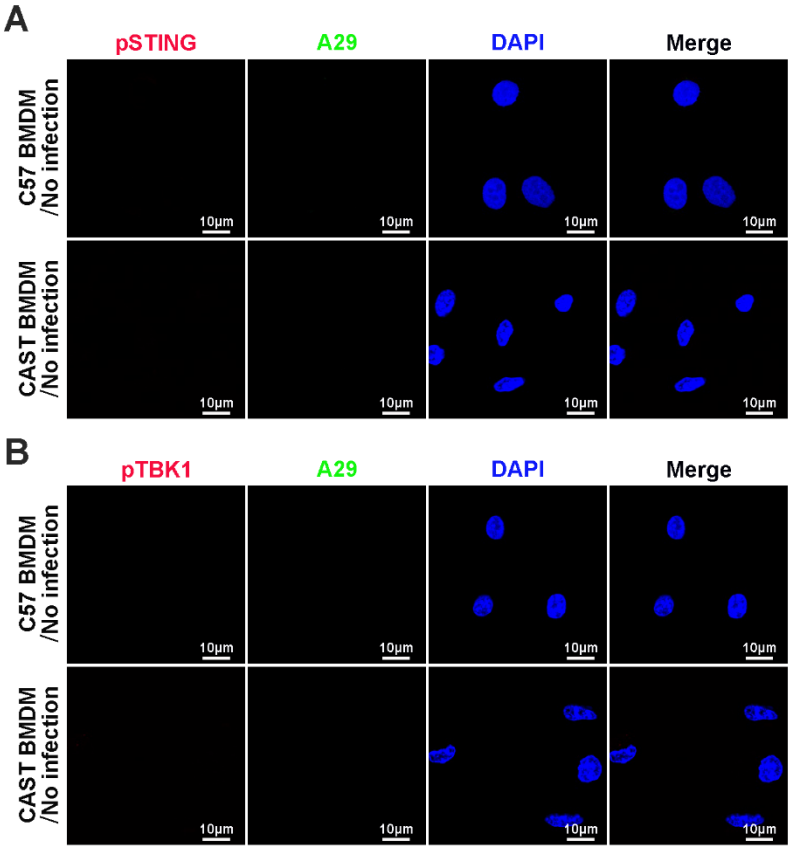

Figure S6 The phosphorylation of pSTING and pTBK1 in BMDMs from C57BL/6J and CAST/EiJ mice was determined through immunofluorescence, Related to Figure 3.
(A, B) BMDMs derived from C57BL/6J and CAST/EiJ mice were immunostained with anti-pSTING (red) (A) or anti-pTBK1 (red) (B) and anti-A29 (green) (A, B) antibodies. The nuclei were stained with DAPI (blue), and images were obtained using a Zeiss LSM 800 Meta confocal microscope.

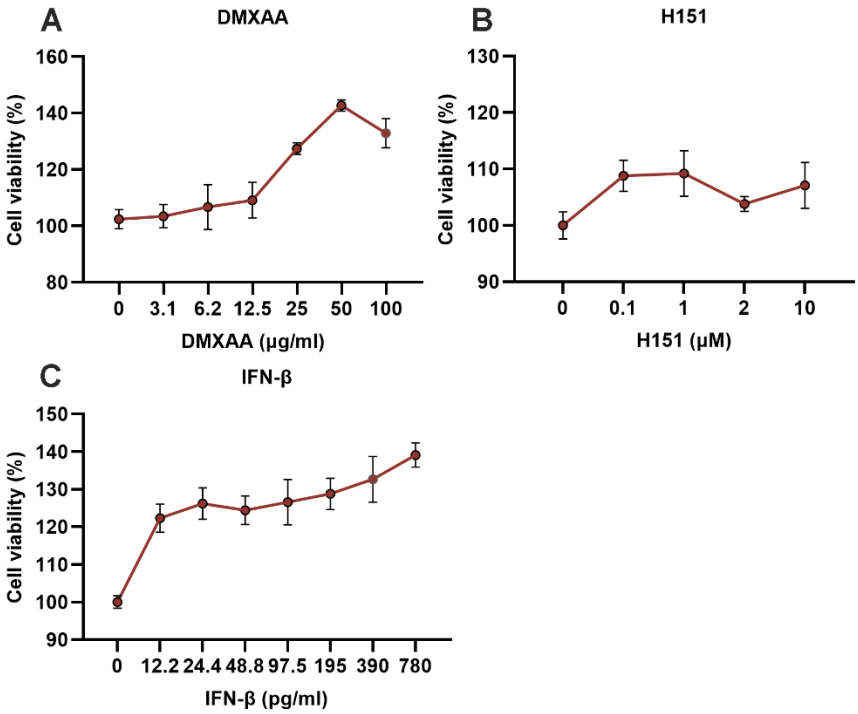

Figure S7 The cytotoxicity of DMXAA, H151, and IFN-β was assessed using the CCK-8 assay, Related to Figure 5.

BMDMs were treated with the indicated concentrations of DMXAA, H151, and IFN-β used in this study. After twenty-four hours, cell viability was measured using the CCK-8 assay. The data are presented as the means ± SEM.

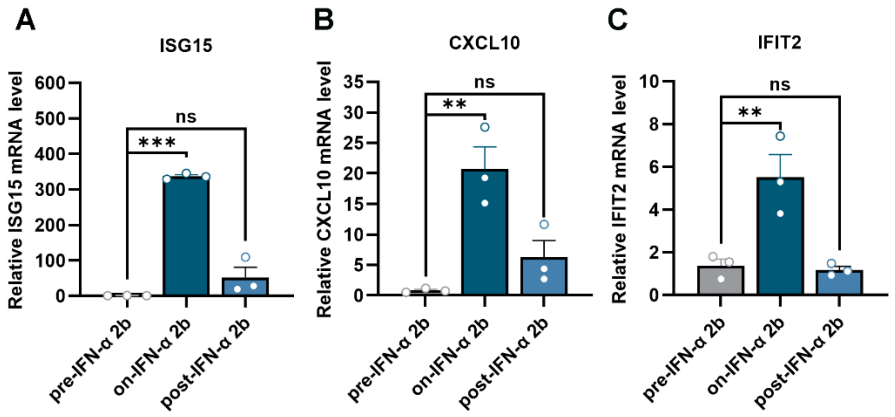

Figure S8 The transcription levels of ISG-related genes in rhesus monkeys PBMCs at different stages of IFN α-2b treatment. Related to Figure 6.

(A-C). PBMCs were derived from rhesus monkeys before (pre-), during (on-), and after (post-) IFN α-2b treatment (one day before IFN α-2b administration, one day post initial IFN α-2b administration, 28 days post initial IFN α-2b administration), and the mRNA expression levels of ISG15 (A), CXCL10 (B), and IFIT2 (C) were quantified by qRT–PCR. Differences between the groups were evaluated using one-way ANOVA (ns, not significant; $^{**}P < 0.01$; $^{***}P < 0.001$). The data are presented as the means ± SEM.

Table S1. Primers used for qRT-PCR. Related to STAR Methods.

Gene Product	Forward primer (5' to 3')	Reverse primer (5' to 3')
mouse-β-actin	TGTTACCAACTGGGACGACA	CTGGGTCATCTTTTCACGGT
mouse-IFN-β	ATGAGTGGTGGTTGCAGGC	TGACCTTTCAAATGCAGTAGATTCA
mouse-CXCL10	ATCATCCCTGCGAGCCTATCCT	GACCTTTTTTGGCTAAACGCTTTC
mouse-ISG15	AGAAGCAGATTGCCCAGAAG	TGCGTCAGAAAGACCTCATAGA
mouse-ISG56	TGCTGAGATGGACTGTGAGGAA	TCTTGGCGATAGGCTACGACTG
mouse-CCL5	CACCACTCCCTGCTGCTTTG	ACACTTGGCGGTTCCTTCG
mouse-IFIT2	GCTCTGGAAAAGGACCCGAA	GCTTCAGTGCCAAGAGGACT
Rhesus Macaques (RM) GAPDH	CTCCTGTTCGAGAGTCAGCC	GGGGCTTCCATTGATGACGA
RM ISG15	GGCAGTTGAGAGGCAGTGAA	TTCTGGGCGATCTTTGCCTT
RM CXCL10	ACTGTACGCTGTACCTGCATC	CAGACACCTCTTCTCACCCTT
RM IFIT2	CTCAGAACGCCATTGACCCT	TCTTCGCCTTCTTCACGCAT
MPXV F3L	CTCCTGTTCGAGAGTCAGCC	GGGGCTTCCATTGATGACGA
MPXV F3L probe	5'-(FAM)-CATCAGAATCTGTAGGCCGT-(MGB)-3'	

Click here to access/download
Highlights and eTOC Blurb
Highlights and eTOC blurb.docx

CellPress

CELL PRESS DECLARATION OF INTERESTS POLICY

Transparency is essential for a reader's trust in the scientific process and for the credibility of published articles. At Cell Press, we feel that disclosure of competing interests is a critical aspect of transparency. Therefore, we require a "declaration of interests" section in which all authors disclose any financial or other interests related to the submitted work that (1) could affect or have the perception of affecting the author's objectivity or (2) could influence or have the perception of influencing the content of the article.

What types of articles does this apply to?

We require that you disclose competing interests for all submitted content by completing and submitting the form below. We also require that you include a "declaration of interests" section in the text of all articles even if there are no interests to declare.

What should I disclose?

We require that you and all authors disclose any personal financial interests (e.g., stocks or shares in companies with interests related to the submitted work or consulting fees from companies that could have interests related to the work), professional affiliations, advisory positions, board memberships (including membership on a journal's advisory board when publishing in that journal), or patent applications and/or registrations that are related to the subject matter of the contribution. As a guideline, you need to declare an interest for (1) any affiliation associated with a payment or financial benefit exceeding $10,000 p.a. or 5% ownership of a company or (2) research funding by a company with related interests. You do not need to disclose diversified mutual funds, 401ks, or investment trusts.

Authors should also disclose relevant financial interests of immediate family members. Cell Press uses the Public Health Service definition of "immediate family member," which includes spouse and dependent children.

Where do I declare competing interests?

Competing interests should be disclosed on this form as well as in a "declaration of interests" section in the manuscript. This section should include financial or other competing interests as well as affiliations that are not included in the author list. Examples of "declaration of interests" language include:

> "AUTHOR is an employee and shareholder of COMPANY."
> "AUTHOR is a founder of COMPANY and a member of its scientific advisory board."

NOTE: Primary affiliations should be included with the author list and do not need to be included in the "declaration of interests" section. Funding sources should be included in the "acknowledgments" section and also do not need to be included in the "declaration of interests" section. (A small number of front-matter article types do not include an "acknowledgments" section. For these articles, reporting of funding sources is not required.)

What if there are no competing interests to declare?

If you have no competing interests to declare, please note that in the "declaration of interests" section with the following wording:

> "The authors declare no competing interests."

CellPress

CELL PRESS DECLARATION OF INTERESTS FORM

If submitting materials via Editorial Manager, please complete this form and upload with your initial submission. Otherwise, please email as an attachment to the editor handling your manuscript.

Please complete each section of the form and insert any necessary "declaration of interests" statement in the text box at the end of the form. A matching statement should be included in a "declaration of interests" section in the manuscript.

Institutional affiliations

We require that you list the current institutional affiliations of all authors, including academic, corporate, and industrial, on the title page of the manuscript. ***Please select one of the following:***

☒ All affiliations are listed on the title page of the manuscript.

☐ I or other authors have additional affiliations that we have noted in the "declaration of interests" section of the manuscript and on this form below.

Funding sources

We require that you disclose all funding sources for the research described in this work. ***Please confirm the following:***

☒ All funding sources for this study are listed in the "acknowledgments" section of the manuscript.*

*A small number of front-matter article types do not include an "acknowledgments" section. For these, reporting funding sources is not required.

Competing financial interests

We require that authors disclose any financial interests and any such interests of immediate family members, including financial holdings, professional affiliations, advisory positions, board memberships, receipt of consulting fees, etc., that:

(1) could affect or have the perception of affecting the author's objectivity, *or*
(2) could influence or have the perception of influencing the content of the article.

Please select one of the following:

☒ We, the authors and our immediate family members, have no financial interests to declare.

☐ We, the authors, have noted any financial interests in the "declaration of interests" section of the manuscript and on this form below, and we have noted interests of our immediate family members.

Advisory/management and consulting positions

We require that authors disclose any position, be it a member of a board or advisory committee or a paid consultant, that they have been involved with that is related to this study. We also require that members of our journal advisory boards disclose their position when publishing in that journal. ***Please select one of the following:***

- ☒ We, the authors and our immediate family members, have no positions to declare and are not members of the journal's advisory board.
- ☐ The authors and/or their immediate family members have management/advisory or consulting relationships noted in the "declaration of interests" section of the manuscript and on this form below.

Patents

We require that you disclose any patent applications and/or registrations related to this work by any of the authors or their institutions. ***Please select one of the following:***

- ☒ We, the authors and our immediate family members, have no related patent applications or registrations to declare.
- ☐ We, the authors, have a patent application and/or registration related to this work, which is noted in the "declaration of interests" section of the manuscript and on this form below, and we have noted the patents of immediate family members.

Please insert any "declaration of interests" statements in this space. This exact text should also be included in the "declaration of interests" section of the manuscript. If no authors have a competing interest, please insert the text, "The authors declare no competing interests."

The authors declare no competing interests.

☒ **On behalf of all authors, I declare that I have disclosed all competing interests related to this work. If any exist, they have been included in the "declaration of interests" section of the manuscript.**